STUDIES ON PREPARATIONS AND PHOTOELECTROCHEMICAL PROPERTIES OF QUANTIZED SEMICONDUCTOR NANOCRYSTALS

1996

HAJIME MATSUMOTO

Department of Applied Chemistry
Faculty of Engineering
Osaka University

STUDIES ON PREPARATIONS AND PHOTOELECTROCHEMICAL PROPERTIES OF QUANTIZED SEMICONDUCTOR NANOCRYSTALS

(量子化半導体超微粒子の調製と光電気化学特性に関する研究)

1996

HAJIME MATSUMOTO

Department of Applied Chemistry
Faculty of Engineering
Osaka University

Preface

The work of this thesis was carried out under the guidance of Professor Dr. Hiroshi Yoneyama at Department of Applied Chemistry, Faculty of Engineering, Osaka University.

The objective of this thesis is to develop preparation methods of size quantized semiconductor nanocrystals of desired sizes, and to investigate the size dependent photoelectrochemical properties of the prepared nanocrystals. The author hopes that the findings obtained in this work will benefit in progress in photochemistry of semiconductor nanocrystals.

Hajime Matsumoto

Department of Applied Chemistry,
Faculty of Engineering,
Osaka University
Yamada-oka, Suita, Osaka 565, Japan
January / 1996

Contents

General Introduction

Semiconductor nanocrystals (Q-particles) with diameters less than ca. 10 nm have been extensively investigated since they exhibit various unique photophysical and/or photochemical properties due to the quantum size effects. The size dependency of the energy structure of the Q-particles have been predicted by various theoretical calculations using the schrödinger equation for electrons in a small space. Various preparation methods of Q-particles have been proposed to investigate the size dependent properties of Q-particles but particles prepared so far had size distribution more or less, which limits studies on size-dependent properties. It is desired to develop a technique that allows the preparation of Q-particles with precisely controlled size and crystalline properties with a high monodispersivity.

Recently, the use of Q-particles as photocatalysts have drawn much attentions because it has been shown experimentally that apparent photocatalytic activities of semiconductor particles increase with a decrease of its size. This phenomena has been qualitatively explained in terms of increase in both the reducing power of photogenerated electrons and oxidizing power of holes due to the enlargement of the bandgap of semiconductors, the degree being dependent on the size of Q-particles.

Q-particles of metal chalcogenide semiconductors such as CdS, and oxide semiconductors such as TiO_2 have most intensively been studied since these Q-particles can be prepared without difficulty. On the other hand, the preparation of III-V compound semiconductors such as GaAs is not easily done, and little studies have been done on their size quantization effects.

The present study has been conducted focusing to the following three subjects.

(1) To clarify the effect of the size of semiconductor nanocrystals on the photoelectrochemical properties of Q-particles.

(2) To develop the preparation method of monodispersed CdS nanocrystals.

(3) To develop the preparation of GaAs nanocrystals

This thesis is composed of the General Introduction, four chapters of the text, and conclusion. Chapter 1 describes the effect of the particle size of Q-CdS on the photo-induced electron transfer to methylviologen and sulfopropylviologen. Q-CdS nanocrystals prepared by applying gel electrophoresis to CdS nanocrystals colloids to narrow the size distribution were used. Chapter 2 describes the method of the determination of the conduction band potential of CdS nanocrystals using TiO_2 colloids as a potential variable quencher. Chapter 3 describes a novel method of the preparation of monodispersed CdS nanocrystals using photoinduced dissolution under aerobic condition. Chapter 4 describes the preparation and characterization of GaAs nanocrystals and the application to the photocatalyst. The conclusion summarizes the results obtained in the present study.

List of Publications

(1) Photoinduced Reaction on Quantized GaAs Nanocrystals Prepared by Wet Process

Hajime Matsumoto, Hiroyuki Uchida, Takao Sakata, Hirotaro Mori, and Hiroshi Yoneyama

Res. Chem. Intermed. **1994**, *20*, 723-733.

(2) Photoinduced Reduction of Viologens on Size-Separated CdS Nanocrystals

Hajime Matsumoto, Hiroyuki Uchida, Takahiro Matsunaga, Koji Tanaka, Takao Sakata, Hirotaro Mori, and Hiroshi Yoneyama

J. Phys. Chem. **1994**, *98*, 11549-11556.

(3) Narrowing Size Distribution of CdS Nanocrystals by Size Selective Photocorrosion

Hajime Matsumoto, Takao Sakata, Hirotaro Mori, and Hiroshi Yoneyama

Chem. Lett. **1995**, 595-596.

(4) Size Dependent Fluorescence Quenching of CdS Nanocrystals Caused by TiO_2 Colloids as a Potential-Variable Quencher

Hajime Matsumoto, Takahiro Matsunaga, Takao Sakata, Hirotaro Mori, and Hiroshi Yoneyama.

Langmuir **1995**, 4283-4287.

(5) Preparation of Monodispersive CdS Nanocrystals by Size Selective Photocorrosion

Hajime Matsumoto, Takao Sakata, Hirotaro Mori, and Hiroshi Yoneyama

J. Phys. Chem. in preparation.

List of Supplementary Publication

(1) Optical Nonlinearity of Quantized GaAs Nanocrystals Prepared by Wet Process

Hajime Matsumoto, Hiroyuki Uchida, Takao Sakata, Hirotaro Mori, Takatomo Sasaki, and Hiroshi Yoneyama

Denki Kagaku **1993**, *61*, 918-919.

Chapter 1 Photoinduced Reduction of Viologens on Size-Separated CdS Nanocrystals

1-1 Introduction

Many workers have described photoinduced electron transfer from size quantized semiconductor particles (Q-particles) to redox species in solution[1-12]. Based on these studies it appears that the rate of photoreduction of a redox species in solution increases as the size of the semiconductor crystallite decreases[2]. This tendency is accounted for by smaller particles having a more negative potential of their conduction band edge[2a,b]. In an electrochemical sense, the potential difference between the conduction band of a semiconductor particle and the redox agent to be photoreduced can be regarded as the overvoltage for electron transfer. However, the enhanced rate with increasing size quantization has not been quantitatively discussed from this viewpoint. The preparation of monodispersed Q-particles with different sizes is desired to investigate this subject.

The rate of the electron transfer from Q-particles is likely to be influenced also by surface composition such as nonstoichiometry[3-6] and the presence of stabilizers[7-9]. Therefore, it is desirable to use Q-particles of different sizes that have been prepared by the same method. In this respect, fractionation by gel electrophoresis[12-14] is suitable for preparation of Q-particles.

In this chapter, the rate of photoinduced reduction of positively charged methylviologen, (MV^{2+}), and electrically neutral propylviologensulfonate, (PVS^{0}), on Q-CdS particles of different sizes, is described. The results obtained are discussed in terms of existing theories of electrochemical reactions.

1-2 Experimental Section

1-2-1 Preparation and Size-Separation of CdS Colloids

Preparation of nanocrystalline CdS colloids followed the method reported by Spanhel *et al.*[15]. A stoichiometric amount of H_2S was injected into a nitrogen-purged aqueous solution containing 0.2 mM $Cd(ClO_4)_2$ and 0.2 mM sodium hexametaphosphate (HMP) at pH 10.0. After vigorously mixing for 1 min, the newly formed colloid was stirred for 10 min at 0℃ and concentrated by a factor of 10 under reduced pressure at 35℃. Concentrated CdS colloids are denoted Q-CdS/HMP.

Gel electrophoresis was carried out employing a procedure similar to that reported by Eychmüller *et al*[12]. A 2.5 % polyacrylamide gel (2.6 % cross-linking density, diameter 25 mm, length 17 cm) was used. Both the gel and the electrolyte solution contained 5 mM $Cd(ClO_4)_2$ and 5 mM HMP at pH 10.9. A Pt plate cathode was placed in the upper reservoir of the electrophoresis cell and a Pt wire anode in the lower reservoir. 10 cm^3 of Q-CdS/HMP containing 10 w/v % sucrose was overlayered on the top of the gel. Electrophoresis experiments were performed by application of 100 V for 4 h. To minimize thermal diffusion of Q-CdS particles in the gel, the electrophoresis cell was cooled in an ice bath. The electrolyte solution was replaced every 30 min to maintain a constant pH. The resulting Q-CdS gel layer of 6 cm length was cut into 6 slices. The fraction close to the cathode (top end) is numbered 1 and the bottom end 6 in this chapter. Using the cell shown in Figure 1-1, electrophoresis was again carried out to extract Q-CdS particles in a given gel slice by putting it on a Nylon sheet separator (400 mesh) wrapping the bottom end of the glass tube. Below the Nylon sheet separator, 5 cm^3 of the electrolyte solution was filled, which was separated from the anode compartment by a cellulose dialysis membrane (Viskase Sales Co. UC36-32). By application of 20 V for 30 min, the Q-CdS particles were extracted from the gel into the electrolyte

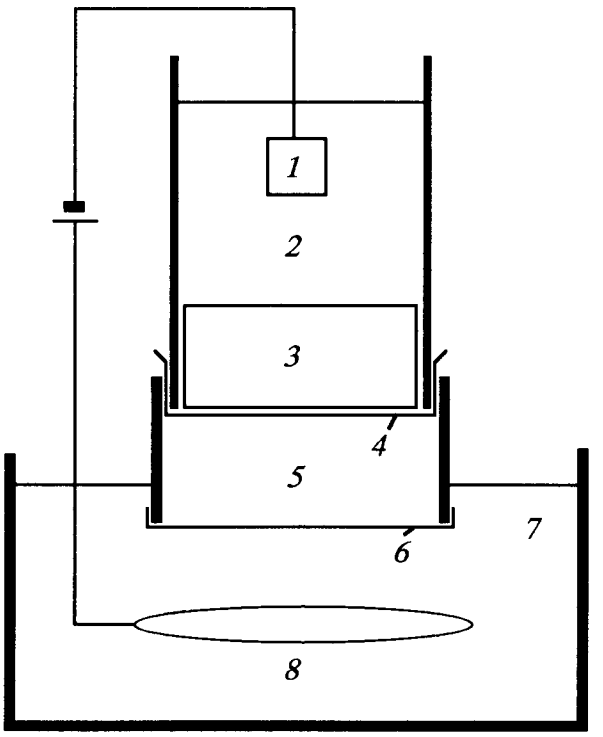

Figure 1-1 Schematic illustration of the cell for electrophoretic extraction of Q-CdS particles from a slice of the gel into the electrolyte solution. *1*: Pt plate (cathode), *2*: cathode compartment, *3*: slice of polyacrylamide gel containing Q-CdS particles, *4*: Nylon mesh separator, *5*: electrolyte container (5 cm^3), *6*: cellulose dialysis membrane, *7*: anode compartment, *8*: Pt wire (anode), *9*: glass tube. The electrolyte solution contained 5 mM $Cd(ClO_4)_2$ and 5 mM HMP at pH 10.9.

solution below the Nylon sheet separator. The resulting colloidal dispersion was filtered using a 0.2 μm PTFE filter (Advantec) to remove the gel, and about 5 cm^3 of the fractionated Q-CdS colloid recovered.

1-2-2 Characterization of Fractionated CdS Colloids

A transmission electron microscope, TEM (Hitachi H800, 200 keV or H9000, 300 keV), was employed to determine the size distribution of the CdS nanocrystallites in each fraction. A small amount of the colloidal solution was dropped onto a carbon-evaporated copper grid for observations. The amount of CdS in each fraction was determined using a fluorescent X-ray spectrometer (Rigaku,

3270A). 0.05 cm^3 of the Q-CdS colloid or standard solutions of various concentrations (Na_2SO_4 for sulfur analysis) was dropped on a filter paper (Rigaku, 3379C1) followed by drying under vacuum. The concentration of CdS was determined by assuming that the fractionated Q-CdS particles were stoichiometric.

Optical absorption and fluorescence spectra of each fraction were measured using a photodiode-array spectrophotometer (Hewlett-Packard, HP8452A) and a fluorescence spectrometer (Hitachi, F3010), respectively. The fluorescence lifetime of the CdS nanocrystallites was determined using a time-resolved single-photon counting method on a fluorescence spectrophotometer (Horiba, NAES-1100).

1-2-3 Photoinduced Reduction of Methylviologen and Propylviologensulfonate in Fractionated CdS Colloidal Dispersions

To keep the number of photons absorbed constant, the absorbance of the fractionated Q-CdS colloid at 355 nm was adjusted to 0.15 by addition of 5 mM HMP solution. The resulting colloid contained 0.1 to 0.2 mM CdS, depending on the size of Q-CdS particles. Methylviologen (Tokyo Kasei) or propylviologensulfonate (Sigma) and EDTA (Dojin) were added to the colloid as an electron acceptor and a hole scavenger, respectively. The pH of the colloid was adjusted to 5 ~ 11 by addition of 1 M NaOH. 3 cm^3 of the colloid was placed into a 1 cm × 1 cm quartz cell. The third harmonic (355 nm) of a Q-switched Nd:YAG laser (Spectra-Physics, GCR-11, beam diameter 8 mm, pulse width 15 ns, beam intensity 5 ~ 50 mW) was used to irradiated the deaerated colloid at a frequency of 10 Hz with magnetic stirring of the suspension. The photoinduced formation of MV^+ or PVS^- was monitored by measuring changes in the absorption spectrum of the colloidal sample using a photodiode-array spectrophotometer. The transient absorption produced by a single pulse was displayed on a digitizing oscilloscope (Hewlett Packard, 54510A, minimum measurement interval = 1 ns). The analyzing light passed through the cell (perpendicular to the laser beam) and a monochromater

(McPherson, 2035) placed in front of a photomultiplier (Hamamatsu, R955). The analyzing source was a 500 W Xenon lamp equipped with pulse generator (Ewig, PG-500), a UV-cut-off filter and a 550 nm cut-off filter. The above configuration transmitted wavelengths longer than 550 nm thereby precluding band gap excitation of the colloidal sample.

1-3 Results and Discussion

1-3-1 Observation of CdS Nanocrystals by TEM

Figure 1-2 shows the TEM picture of unfractionated Q-CdS/HMP taken by using H9000 with the accelaration voltage of 300 keV. The figure clearly indicated the obtained CdS particles have a spherical shape. The size of Q-CdS estimated by

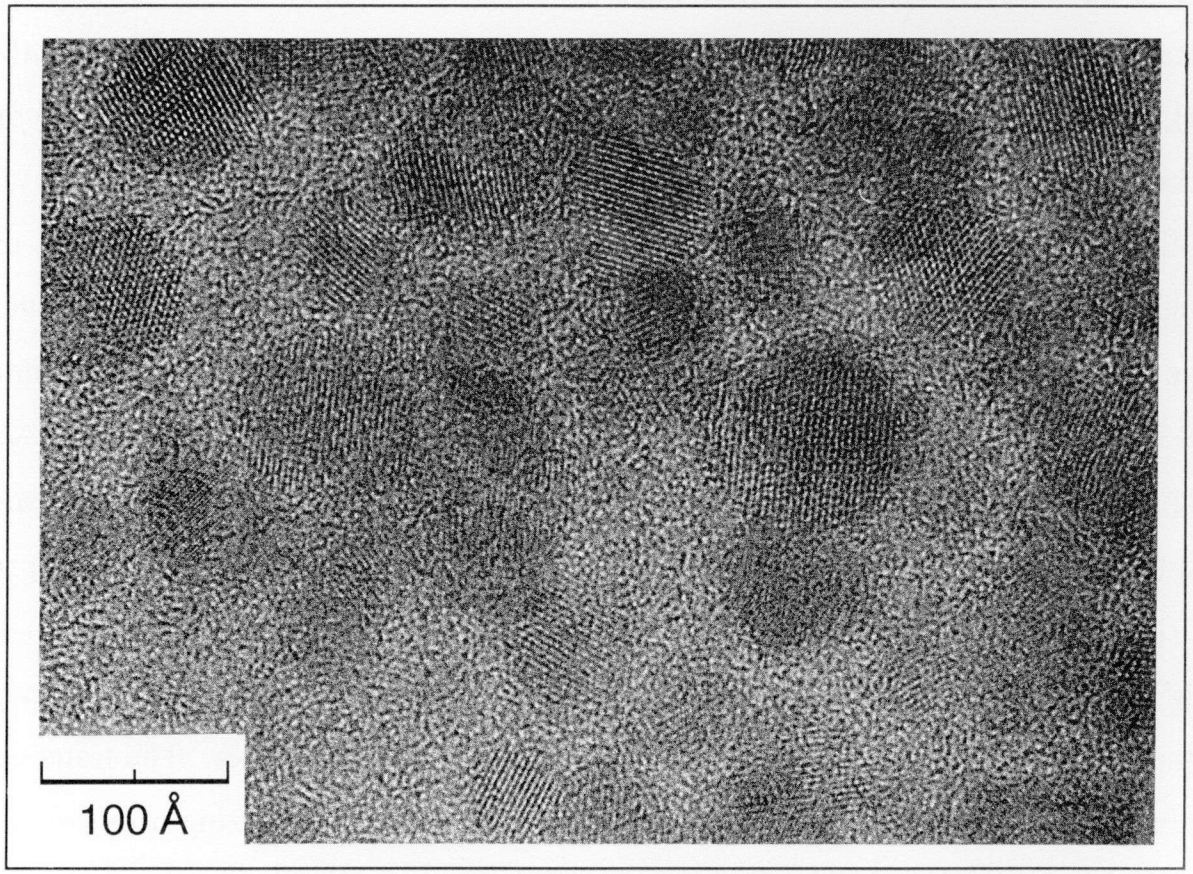

Figure 1-2 TEM image of CdS nanocrystals. Accelaration voltage: 300 keV

the TEM picture ranges from 3 to 8 nm (an average diameter of 4.40 nm, standard deviation 1.30 nm). The electron diffraction patterns simultaneously obtained with TEM indicated that the crystal structure of Q-CdS was a zinc-blende structure.

1-3-2 Size-Separation of CdS Colloids

Use of electrophoresis permitted efficient and prompt extraction of Q-CdS particles as compared with previously reported procedures[12,13] in which a slice gel was placed in electrolyte solution overnight. Figure 1-3 shows the absorption spectra of fractions 1 ~ 6 together with that of the unfractionated Q-CdS/HMP. The absorption onset of the unfractionated Q-CdS/HMP is 513 nm. Following size-separation by electrophoresis, the absorption spectrum blue-shifted and became

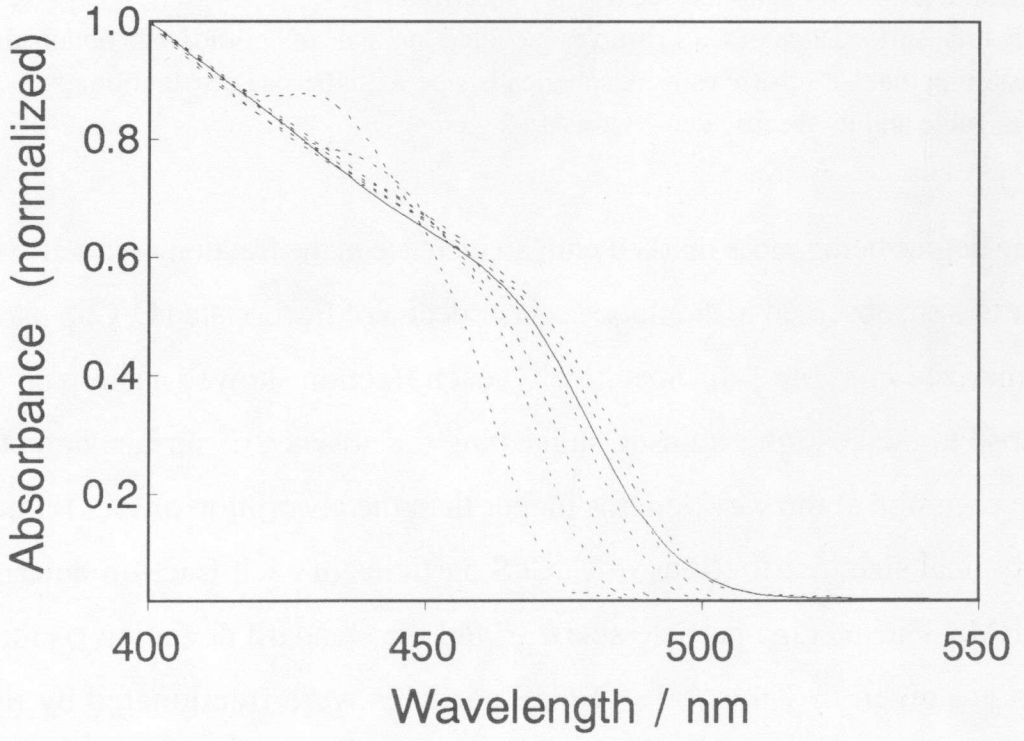

Figure 1-3 Absorption spectra of the unfractionated colloid (solid line, absorption onset = 510 nm) and of fractions 1 ~ 6 (dashed lines, from right to left). The spectra were normalized at 400 nm.

Table 1-1 Physical and optical properties of the fractionated CdS colloids

fraction no.	absorption onset[a] (nm)	fluorescence maximum (nm)	$E_g(r)$[b] (eV)	d_{av}[c] (nm)	σ_d[d] (nm)	d_{cal}[e] (nm)	[CdS][f] (mM)	total surface area[g] (cm^2)
1	498	490	2.49	5.01	0.96	5.6	0.178	192
2	494	488	2.51	4.57	1.06	5.2	0.172	203
3	489	484	2.53	4.01	0.73	4.8	0.172	232
4	486	481	2.55	3.61	0.63	4.6	0.188	281
5	484	475	2.56	3.37	0.67	4.5	0.208	333
6	474	468	2.61	2.94	0.53	4.0	0.146	268

[a] Determined from $(\varepsilon h\nu)^2$ *vs.* $h\nu$ plots for the adsorption spectrum.

[b] Representative bandgap from the absorption onset.

[c] Average diameter determined from TEM pictures.

[d] Standard deviation of the diameter determined from TEM pictures.

[e] Determined by appling $E_g(r)$ to a reported energy gap *vs.* particle diameter relation [17].

[f] The concentration of CdS included in the colloids was adjusted so as to give the absorbance of 0.15 at 355 nm for all cases. [CdS] was estimated from the amount of sulfur determined by a fluorescent X-ray spectrometry.

[g] The total surface area of CdS particles included in 3 cm^3 of colloids was obtained by assuming that CdS particles were spherical shape with the size distribution given in this Table and its specific density was 4.82 g cm^{-3}.

steep, the degree being more marked with an increase in the fraction number. Similar blue-shifts were observed in the fluorescence spectra of fractionated Q-CdS particles, as summarized in Table 1-1. Specifically, each fraction showed a sharp emission band close to the absorption onset, suggesting the absence of surface defects that give the emission at the wavelengths longer than the absorption onset. Figure 1-4 shows typical size distributions of Q-CdS particles in each fraction determined from TEM. The average particle size d_{av} and the standard deviation σ_d for each fraction are given in Table 1-1. Q-CdS particles were fractionated by the gel electrophoresis as expected. The average diameter of Q-CdS particles present in fraction 1 was 5.01 nm, while that in fraction 6 was 2.94 nm. In the present study, fractionated Q-CdS particles were prepared using several Q-CdS gel layers prepared under the same electrolysis conditions. However, the fractionated Q-CdS particles

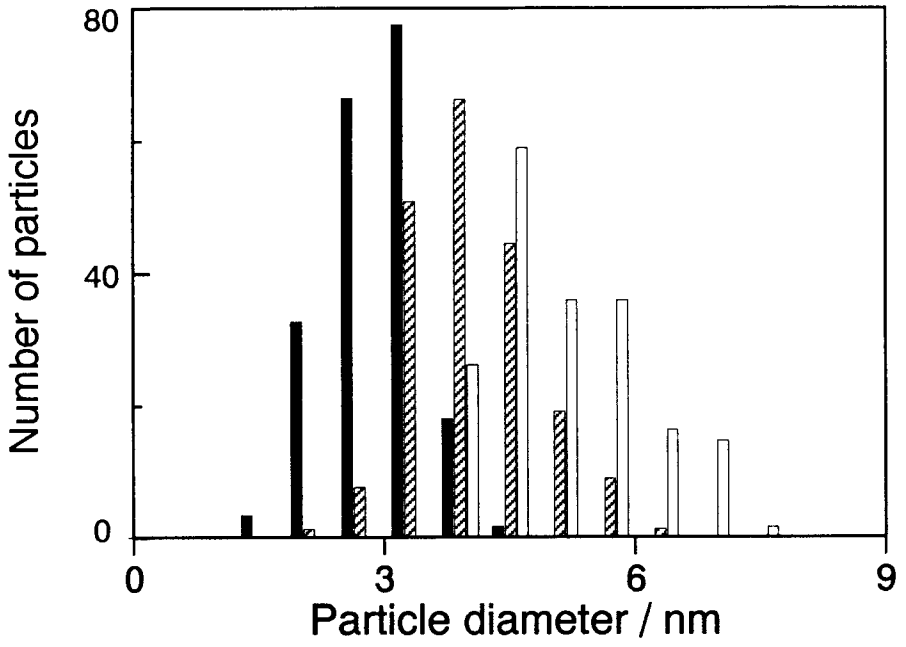

Figure 1-4 Size distributions of CdS microcrystals fractionated by the electrophoresis. (empty bar) fraction 1; (hashed bar) fraction 3, (filled bar) fraction 6.

obtained did not always give the same averaged size for the same numbered fractions. The results given in Table 1- 1 are those obtained for one Q-CdS gel layer, but in experiments of photoinduced electron transfer, which will be described below, fractionated Q-CdS particles prepared with use of three different Q-CdS gel layers were used.

Since Q-CdS particles in each fraction also has a size-distribution, the band gap E_g has a corresponding distribution. Therefore the band gap $E_g(r)$ for each fraction is determined by fitting eq. 1-1 to tails of the obtained absorption spectra,

$$(\varepsilon h\nu)^2 = A\,[h\nu - E_g(r)] \qquad (1\text{-}1)$$

where ε is the absorption coefficient and $h\nu$ is the photon energy.
Although the above equation is valid for bulk semiconductors, plots of $(\varepsilon h\nu)^2$ against $h\nu$ for Q-CdS particles also give a straight line. $E_g(r)$ thus obtained is a measure of the energy gap of the largest CdS particles in each fraction, the optical absorption threshold of the colloids being determined by the largest particles present in a

gigantic fraction[16a,b]. The diameter d_{cal} of Q-CdS particles estimated from a theoretically derived E_g *vs.* particle diameter relation[17] is in good accord with (d_{av} + σ_d) given in Table 1-1 for each fraction.

Table 1-1 also summarizes the concentration and the total surface area of the fractionated Q-CdS particles present in a 3 cm^3 of a quartz cell. As stated, the absorption at 355 nm was adjusted to 0.15. It was shown by fluorescence X-ray spectroscopy that if this absorbance adjustment was made, the concentration of CdS was almost the same in each fraction. The total surface area of the Q-CdS particles present in the quartz cell was determined from the CdS concentration, the density of zinc-blende CdS crystal and the size distribution of particles.

1-3-3 Effects of Surface Layer of Q-CdS on Charge Transfer

Photoinduced formation of MV^+ was evident from the characteristic absorption band of MV^+ superimposed on the Q-CdS spectrum. The absorption band assigned to the MV^+ dimer[4,10] $(MV^+)_2$ was not observed under our experimental conditions. It was also confirmed that MV^{2+} and EDTA effectively scavenged electrons and holes, respectively, without any photodegradation of Q-CdS. Specifically the absorption tail of Q-CdS remained unchanged during illumination. The time course of the absorbance change at 606 nm caused by the illumination is shown in Figure 1-5. From its initial slope and the molar absorption coefficient at 606 nm (ε = 13700 M^{-1} cm^{-1} [18]), the initial rate of formation of MV^+ was determined under various concentration of MV^{2+} and EDTA. The initial rate of MV^+ production using unfractionated Q-CdS colloids at fixed EDTA concentration increased with increasing MV^{2+} concentration and leveled off at about 1 mM of MV^{2+}. The experimental conditions were the same as those given in the caption of Figure 1-5 except for [MV^{2+}]. This result suggests that the amount of adsorbed MV^{2+} saturates under such conditions as already reported for the MV^{2+} - CdS colloid system[7]. It was also found that for fixed MV^{2+} concentration of 1 mM, the concentration of

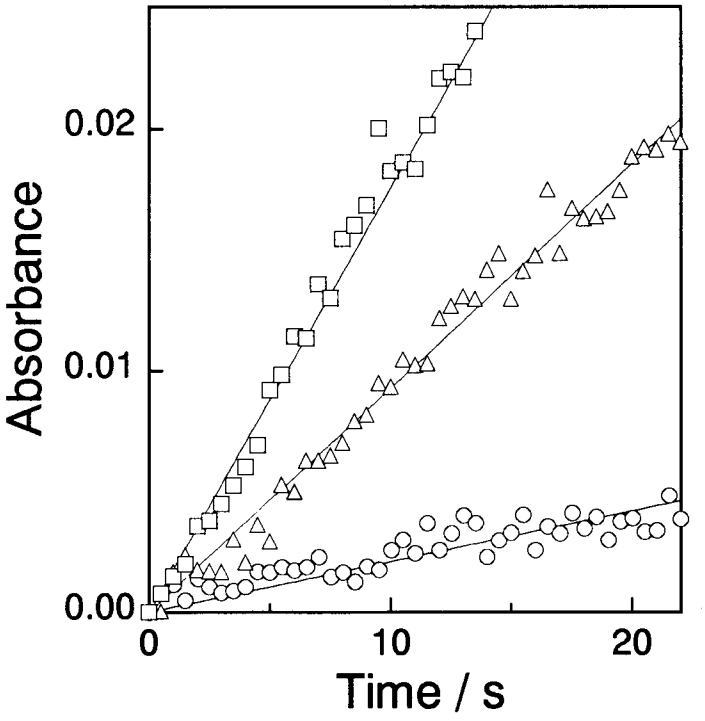

Figure 1-5 Time course of absorbance change at 606 nm for the fraction 1 (○), 4 (△), 6(□), containing MV^{2+}, EDTA and excess Cd^{2+}, caused by repetitive illumination with laser pulses (355 nm, repetition frequency of pulse = 10 Hz, light intensity = 25 mW), $[MV^{2+}]$ = 1 mM, [EDTA] = 1 mM, pH = 11.0, excess $[Cd^{2+}]$ = 5 mM. Absorbance at 355 nm was adjusted to 0.15.

EDTA did not affect the initial rate of MV^{+} production as long as it was equal to or greater than 1 mM. Based on this finding the concentration of EDTA of 1 mM was chosen for studies on the photoinduced reduction of MV^{2+} which are described below.

As shown in Figure 1-6, the rate of reduction of methylviologen was enhanced by increasing solution pH in the absence of Cd^{2+} ions. A greater enhancement was observed in the presence of Cd^{2+}. Inspection of the dependence of the production rate of MV^{+} on the concentration of the added Cd^{2+}, $[Cd^{2+}]_{ad}$, revealed that the rate leveled off at $[Cd^{2+}]_{ad}$ of about 5 mM at pH 11. The absorption spectrum of each Q-CdS fraction remained unchanged following the addition of Cd^{2+} ions, thus it appears that added Cd^{2+} ions do not cause any appreciable increase in the particle size. It has been reported that Q-CdS colloids prepared under excess of either S^{2-} or Cd^{2+} ions exhibit a higher electron transfer rate to MV^{2+} than

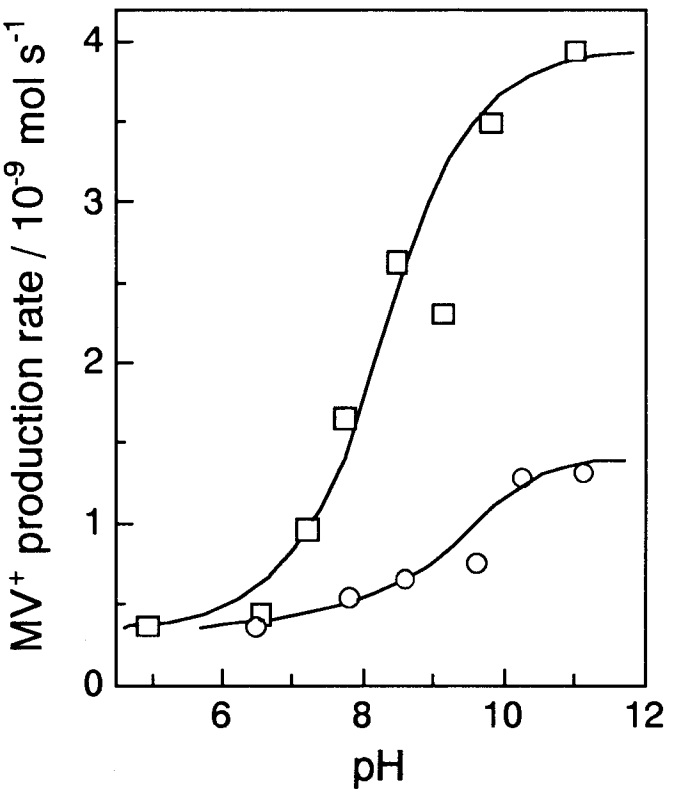

Figure 1-6 pH-dependence of photoinduced production rate of MV^+ for the unfractionated Q-CdS colloids with (□) and without (○) addition of 5 mM Cd^{2+}. [CdS] = 0.06 mM, [MV^{2+}] = 1 mM, [EDTA] = 1 mM. Light source : 500-W Xe lamp (<330 nm and infrared light were cut-off by glass filters).

stoichiometric colloids. It has been suggested that this is due to formation of a MV^{2+}-S^{2-}complex[3] upon addition of S^{2-} ions, or formation of electron trap sites at Q-CdS particle surfaces upon addition of Cd^{2+} ions[4]. It has also been suggested that high activities of ZnS nanocrystallites for photoreduction of CO_2 is a consequence of a nonstoichiometric surface composition [5,6]. However, the pH effect observed here seems not to be related to surface nonstoichiometry of Q-CdS particles, because it is unlikely that changes in solution pH would cause any significant changes in the surface composition of Q-CdS particles.

Gutiérrez and Henglein observed enhancement of MV^{2+} reduction following addition of Cd^{2+} ions to CdS colloids. This effect was attributed to catalytic action of metallic cadmium deposited on semiconductor particle surfaces[19]. If this was seen in the case here, the fluorescence of the Q-CdS colloids ought to be quenched by the addition of Cd^{2+} ions. However, the results obtained in the present study

Table 1-2 Fluorescence intensity and maximum wavelength λ_{max} of the unfractionated CdS at room temperature with and without addition of Cd^{2+} at pH 6.5 and pH 11.0.

	pH 6.5			pH 11.0		
$[Cd^{2+}]_{ad}$[a] (mM)	absorption onset (nm)	fluorescence intensity[b]	λ_{max} (nm)	absorption onset (nm)	fluorescence intensity[b]	λ_{max} (nm)
0	509	1	504	509	4	499
5	508	42	503	508	1880	492

[a] The concentration of $Cd(ClO_4)_2$ added to the unfractionated CdS colloid ([CdS] = 0.6 mM). [b] The relative intensity to that of the colloid before the addition of Cd^{2+} at pH 6.5. Excitation wavelength = 360 nm.

(Table 1-2) suggest added Cd^{2+} ions activate emission at wavelengths close to the absorption onset, especially at high pH. Further the emission peak is slightly blue-shifted by the addition of Cd^{2+} ions. Therefore, It is concluded that deposited cadmium metal, if any, does not play an important role in enhancement of the rate of MV^{2+} reduction. With increasing pH, Cd^{2+} ions are more easily converted to $Cd(OH)_2$[20]. The surface Cd^{2+} site on Q-CdS must also be covered with $Cd(OH)_2$ under existing of excess Cd^{2+} ions. If it is assumed that the $Cd(OH)_2$ formed on CdS surfaces blocks radiationless recombination sites at the surface, as discussed by Spanhel *et al.*[15], the observed enhancement of both the reduction rate of MV^{2+} and the fluorescence intensity can be explained.

Although different lifetimes of photoexcited carriers have been reported for different sizes of Q-CdS particles[21-23], the surface conditions of these particles were not always identical. This is because the size was controlled not by pH and excess Cd^{2+} ions, but by changing the preparation conditions. In order to obtain information concerning the size-dependence of photoexcited carrier lifetime in fractionated Q-CdS particles, I monitored fluorescence decay in the presence of 5 mM Cd^{2+} at pH 11. The emission decayed in a multiexponential manner[11,21], which results from dispersion of the rate of electron release into the conduction band from traps present with energy distribution below the conduction band[14,22].

Analysis of the decay data was by a nonlinear least-squares fit to a three-component decay using eq. 1-2.

$$F(t) = a_1 \exp(-t/\tau_1) + a_2 \exp(-t/\tau_2) + a_3 \exp(-t/\tau_3) \quad (1\text{-}2)$$

Since this procedure gave random weighted residuals, χ^2, a little greater than unity, analysis using the larger number of component decay might yield a better fit. However, the fluorescence spectrophotometer used in the present study did not allow such multi component analysis. Nevertheless, the results obtained in the three component decay analysis give rough idea on the distribution profiles of traps. The traps are roughly classified into three different energy levels. The shorter the lifetime the shallower the traps. A relative quantum yield q_i (i = 1~3) for each component, which is a measure of its contribution to the emission a_i (i = 1~3), was also obtained by eq. 1-3.

$$q_i = a_i \tau_i \Big/ \sum_{i=1}^{i=n} a_i \tau_i \quad (n=3) \quad (1\text{-}3)$$

The fitting parameters obtained for each fraction are summarized in Table 1-3. The existence of very shallow electron traps having a depth of few meV below the conduction band of Q-CdS particle accounts for the multi-exponential fluorescence decay[14,22]. Average fluorescence decay, $\langle\tau\rangle$, for such a dispersive rate model can be estimated using eq. 1-4[11,24] in which the τ_i values given in Table 1-3 were used.

$$\langle\tau\rangle = \sum_{i=1}^{i=n} a_i \tau_i^2 \Big/ \sum_{i=1}^{i=n} a_i \tau_i \quad (n=3) \quad (1\text{-}4)$$

$\langle\tau\rangle$ for each fraction was found to be independent of particle size and ranged between 40 and 47 ns. Since none of the above parameters show a definite size-dependence, it is suggested that the surface conditions of the fractionated Q-CdS particles are almost the same, this situation being favorable for investigation on the relationship between particle-size and the rate of photoinduced reduction of MV^{2+} as well as of PVS^0. Hereinafter, I used each fraction of Q-CdS particles at pH 11 with addition of 5 mM Cd^{2+}.

Table 1-3 Multiexponential-fit parameters of Eq. (1-2) and (1-3) for emission decay of fractionated Q-CdS.

frac-tion no.	$E_g(r)$ (eV)[a]	component 1 a_1	τ_1 (ns)	q_1 (%)	component 2 a_2	τ_2 (ns)	q_2 (%)	component 3 a_3	τ_3 (ns)	q_3 (%)	$\chi^{2\,b}$
1	2.49	0.081	3.4	17	0.036	19.4	43	0.0068	96.6	40	1.08
2	2.51	0.080	4.2	23	0.033	19.5	44	0.0054	87.9	33	1.23
3	2.53	0.126	3.5	16	0.058	19.2	42	0.0122	92.3	42	1.06
4	2.55	0.095	4.1	19	0.041	21.5	43	0.0076	100	37	1.34
5	2.56	0.091	4.2	19	0.040	21.8	44	0.0078	91.6	36	1.09
6	2.61	0.127	4.3	15	0.076	24.9	53	0.0107	107	32	1.27

[a] Representative bandgap for each fraction of Q-CdS particles determined from the absorption onset. [b] Random weighted residuals for nonlinear least-squares procedures.

Interaction between semiconductor nanocrystals and electron acceptors plays an important role in photo-induced electron transfer in solution[7]. Information concerning the degree of interaction can be obtained from fluorescence quenching experiments in which the electron acceptor acts as a quencher[25]. The relative fluorescence intensity, I_0/I, of unfractionated Q-CdS particles increases remarkably with an increase in $[MV^{2+}]$ as shown in Figure 1-7(a). Perrin plots of ln (I_0/I) *vs* $[MV^{2+}]$, given in the inset of the same figure, indicate that quenching of Q-CdS particles by MV^{2+} is static. This finding is consistent with Langmuir-type adsorption of MV^{2+} on Q-CdS particles. On the other hand, fluorescence quenching at Q-CdS particles by PVS^0 gives a linear Stern-Volmer relation with low concentration dependence of PVS^0. Further, similar results were obtained for Q-CdS particles of different sizes as shown in Figure 1-7(b). The Stern-Volmer constant (K_{sv}) obtained was 350 M^{-1}. The quenching constant, k_q, obtained by dividing K_{sv} by the average fluorescence lifetime, $<\tau>$, yields as a size independent value of *ca.* $\sim 10^{10}$ M^{-1} s^{-1}. These results show that quenching of Q-CdS particles by PVS^0 is dynamic. The quenching rate appears to be governed by diffusion of PVS^0.

MV^{2+} and PVS^0 influenced fluorescence decay. Relative average fluorescence lifetime $<\tau^0>/<\tau>$ was almost the same as that of I^0/I if the concentration of quencher was the same. This suggests that Stern-Volmer constant obtained by the steady

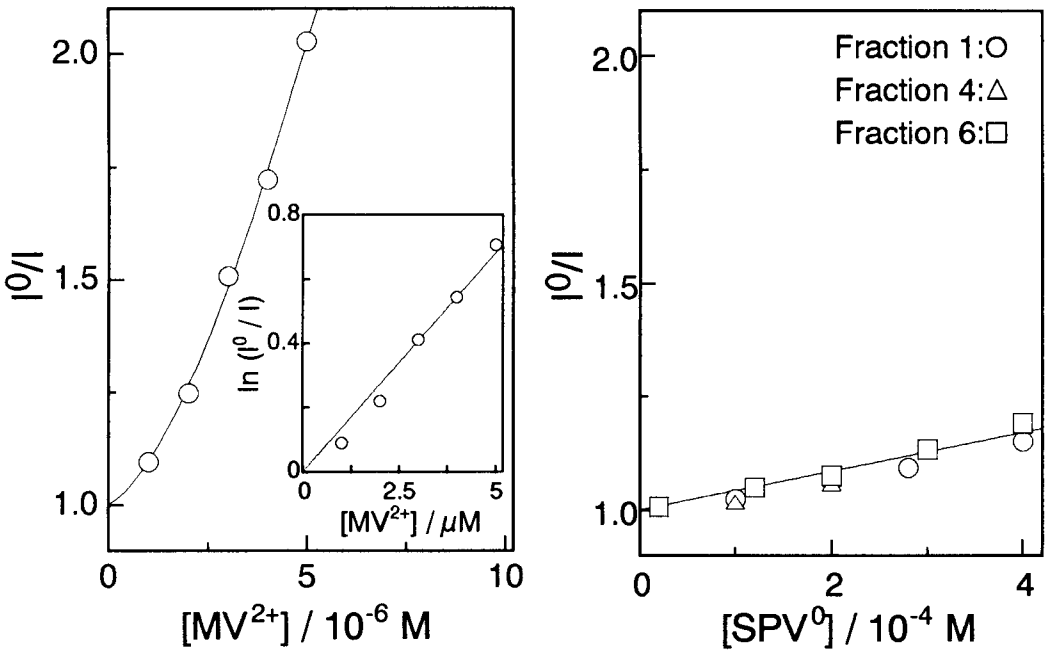

Figure 1-7 Stern-Volmer plot of Q-CdS fluorescence quenching at pH 11.0. (a) unfractionated Q-CdS (absorbance of excitation wavelength, A_{ex} = 0.1). Quencher : MV^{2+}. Insert shows ln (I_0/ I) *vs* [MV^{2+}] plot. (b) fractionated Q-CdS (A_{ex} = 0.15). Quencher : PVS^0. Excitation wavelength is 360 nm in both cases.

state fluorescence intensity represents an average value of those derived from various components. However, if a relation between relative fluorescence lifetime of each component, τ_i^0/τ_i (i=1~3), and the concentration of quencher is obtained, it is found to be different between the two kinds of quenchers, due probably to difference in the quenching process.

1-3-4 Comparison of Photoinduced Charge Transfers between MV^{2+} and PVS^0

Transient absorbance changes, due to formation of reduced viologen, were measured using unfractionated Q-CdS colloids (2 mM) having a CdS particle whose concentration was about 12 times greater than that of the fractionated sample. Results obtained are shown in Figure 1-8. Transient absorbance changes for fractionated Q-CdS colloids could not be obtained. This was because, due to low concentrations of Q-CdS, absorbance changes were below my detection threshold. As shown in

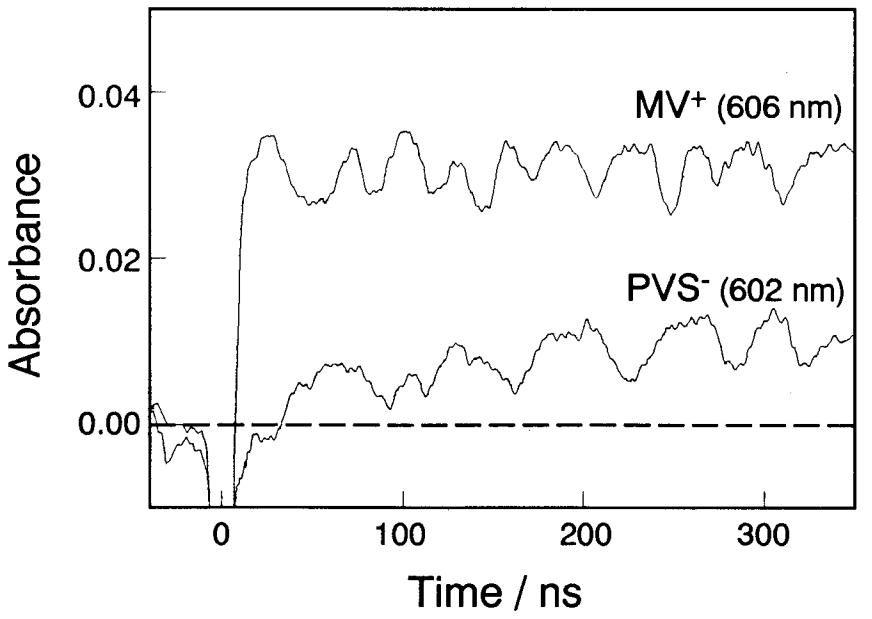

Figure 1-8 Transient absorption at 606 nm (MV^+) and 602 nm (PVS^-) following 355 nm (400 mW) excitation of unfractionated Q-CdS colloid (2 mM) at pH 11.0 containing 1 mM of viologens and EDTA.

the Figure 1-8, a pronounced difference in the growth of the transient absorbance is seen for the two viologens. The formation of MV^+ occurred within the pulse as previously reported for Q-CdS-MV^{2+} systems[4,10]. The absorbance due to the produced MV^+ did not decay during the interruption of irradiation (0.1 sec). In contrast, absorbance of PVS^- increased slowly after pulse irradiation. It is suggested from these results that photoreduced MV^{2+} is adsorbed MV^{2+}, while photo-reduction of PVS^0 is diffusion limited. These findings are in good agreement with the results of the fluorescence quenching experiments as stated in 1-3-3.

Upon evaluation of the dependence of the rate of photoinduced electron transfer on Q-CdS particle sizes, surface area must be taken into account. The rate of formation of MV^+ or PVS^- per unit surface area of the CdS particles, r_{init}, was determined by dividing its initial rate, which was obtained from the time course of their productions as shown in Figure 1-5, by the total surface area of the particles given in Table 1-1. The dependence of r_{init} on the average particle size for the two kinds of viologens obtained in this way is shown in Figure 1-9. For the case of

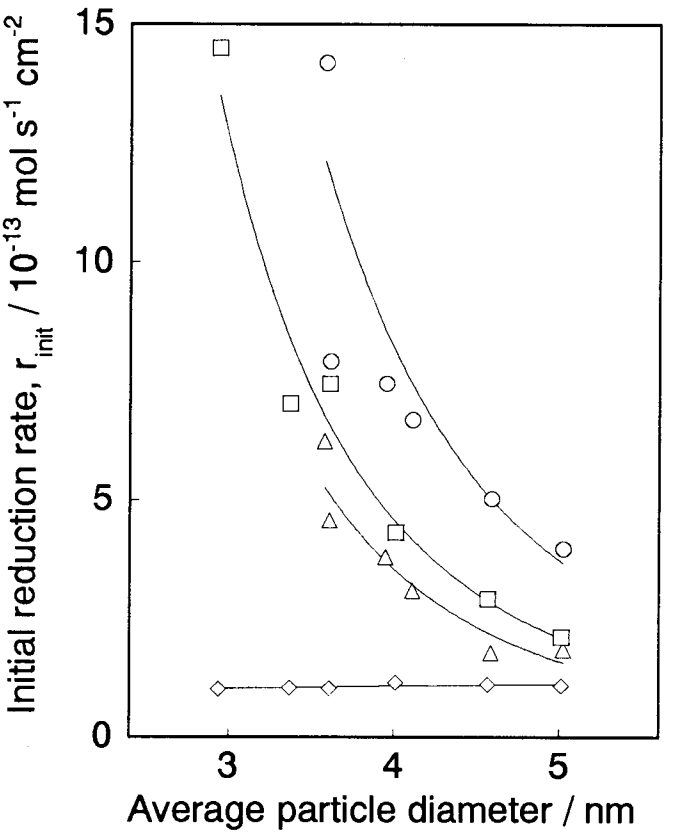

Figure 1-9 Size-dependence of photoinduced production rate of MV^+ per unit surface area of fractionated CdS at pH 11.0. $[MV^{2+}] = [PVS^0] = 1$ mM, [EDTA] = 1 mM, excess $[Cd^{2+}] = 5$ mM. The absorbance of each fraction was adjusted to be 0.15 at 355 nm. Light intensity; (△): 5 mW, (□): 25 mW, (○): 50 mW, (◇): 25 mW (PVS^0).

photo-induced reduction of MV^{2+}, the smaller the particle size, the faster the rate of formation of MV^+, while almost constant r_{init} was obtained for all fractions for photoreduction of PVS^0. Furthermore, the r_{init} of PVS^0 was smaller than that of MV^{2+}, see Figure 1-9. Such results are consistent with diffusion limited photoreduction of PVS^0.

1-3-5 Analysis of Size-Dependence of the Rate of Charge Transfers to MV^{2+}

It is likely that several reactions occur competitively in photoreduction of MV^{2+} on illuminated Q-CdS particle surfaces. As already stated, only adsorbed MV^{2+} is involved in the photo-induced reaction.

excitation: $CdS + h\nu \xrightarrow{g} e^- + h^+$ (1-5)

recombination: $e^- + h^+ \xrightarrow{k_r} CdS$ (1-6)

MV^{2+} reduction: $MV^{2+}_{ad} + e^- \xrightarrow{k_{et}} MV^+_{ad}$ (1-7)

back reaction: $MV^+_{ad} + h^+ \xrightarrow{k_b} MV^{2+}$ (1-8)

EDTA oxidation: $EDTA + h^+ \xrightarrow{k_h} EDTA^+$ (1-9)

As mentioned above, r_{init} of MV^+ production increased with decreasing the particle size. Reflecting this, the quantum yield increased with decreasing the particle size, as shown in Table 1-4. The quantum yield was influenced also by the intensity of irradiation, the lower the intensity the greater the quantum efficiency. These results are consistent with those reported by Nosaka *et al* [2c] who used thiol-modified Q-CdS particles of various sizes. These workers did not correct for surface area difference between the particles. As shown in Table 1-4, the quantum yields obtained are very low. Since the rate of photogeneration of charge carriers is high, about

Table 1-4 Absorption rate of photons per unit volume of Q-CdS[a] at 25 mW irradiation of 355 nm laser, the quantum efficiency for MV^+ production and number of electron-hole pairs produced in one Q-CdS particles by one pulse excitation[b] at 50 mW, 25 mW and 5 mW.

fraction no.	rate of absorption[a] at 25 mW (mmol cm^{-3} s^{-1})	ϕ(%)[b] and ($<x>_0$[c])		
		at 50 mW	at 25 mW	at 5 mW
1	8.08	0.13 (74)	0.18 (32)	0.65 (7.8)
2	8.37	0.20 (54)	0.26 (25)	0.75 (5.3)
3	8.37	0.26 (42)	0.44 (17)	1.30 (3.5)
4	7.65	0.34 (34)	0.92 (11)	1.87 (3.5)
5	6.95	0.36 (28)	1.04 (8)	2.23 (2.6)
6	9.84	0.61 (28)	1.72 (8)	2.90 (2.4)

[a] The rate of photon absorption per unit volume of Q-CdS was calculated by dividing the number of photons absorbed by each fraction of Q-CdS (absorbance = 0.15 at 355 nm) by the volume of Q-CdS particles included in the illuminated region (beam diameter = 8 mm, path length = 1 cm). [CdS] given in Table 1-1 was used to determine the volume of CdS. [b] Quantum efficiency for MV^+ production. [c] The number of electron-hole pairs produced in one Q-CdS particle, which was calculated by dividing the rate of photons absorption by the number of Q-CdS partilces contained in unit volume of Q-CdS colloid.

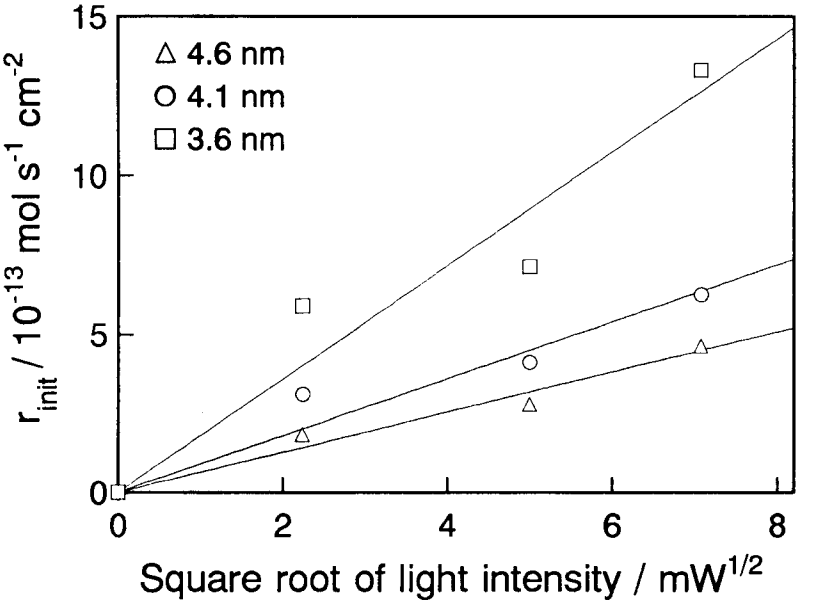

Figure 1-10 Plots of r_{init} *vs.* square root of light intensity at different particle sizes prepared by using the data in Figure 1-9.

0.018 mole photons per second for illumination at 50 mW, recombination of photogenerated charge carriers (eq. 1-6) must be dominant. In that case, the reduction rate does not increase in proportional to the light intensity but to the square root of the light intensity[26], as shown in Figure 1-10 which is prepared using the data given in Figure 1-9. The quantum yields ϕ for MV^{2+} reduction is given by eq. 1-10, where g is the rate of photon absorption, [mol cm^{-3} sec^{-1}], which is proportional to light intensity and independent of particle size, S(D) is total surface area and V is total volume of Q-CdS particles.

$$\phi = \frac{r_{init} \times S(D)}{g\ V} \qquad (1\text{-}10)$$

In my experimental conditions, r_{init} is proportional to $g^{1/2}$ as Figure 1-10 shows, then ϕ is inversely proportional to $g^{1/2}$. This would explain the tendency that the lower the intensity the greater the quantum efficiency. While the maximum absorbance at 606 nm following 355 nm pulsed irradiation appeared within 15 ns-pulse and remained constant during the pulse interval (0.1 sec) as mentioned above, the back electron transfer, eq. 1-8, seems negligible. Then r_{init} is given by eq. 1-11.

$$r_{init} = k_{et} [MV_{ad}^{2+}] [e^-] \quad (1\text{-}11)$$

where $[MV_{ad}^{2+}]$ is the surface concentration of adsorbed MV^{2+} per unit surface area of Q-CdS particles [mol cm^{-2}] and $[e^-]$ is the concentration of photogenerated electrons [mol cm^{-3}].

The concentration of Q-CdS in each fraction was adjusted so as to give the same absorbance at 355 nm. Therefore the number of photons absorbed per unit volume of the CdS particle colloid, g, was almost the same provided the intensity of irradiation was the same (see Table 1-4). Then the concentration of photoexcited electrons in Q-CdS can be regarded to be constant. However, the number of electron-hole pairs produced in one semiconductor particle by one pulse excitation, $\langle x \rangle_0$, is different among each fraction, as shown in Table 1-4. This is because the number of Q-CdS particles becomes great with decreasing the particle size. Rothenberger *et al* have revealed that the recombination dynamics and carrier lifetime are affected by the $\langle x \rangle_0$[27]. They derived a relationships between the carrier lifetime, $\tau_{1/2}$, and $\langle x \rangle_0$, as given by eq. 1-12,

$$\tau_{1/2} = \frac{\alpha\, V(D)}{\langle x \rangle_0\, k_r} \qquad \begin{array}{l} \langle x \rangle_0 < 30 \text{ for } 0<\alpha<1 \\ \langle x \rangle_0 \geq 30 \text{ for } \alpha=1 \end{array} \quad (1\text{-}12)$$

where V(D) is the volume of one CdS particle, k_r is the second order rate constant for carrier recombination [$cm^3 sec^{-1}$], and α depends on $\langle x \rangle_0$ and is obtained from Figure 4(a) of Ref. 27.

The fluorescence lifetime measurements were carried out under low excitation intensity which may correspond to $\langle x \rangle_0 << 1$, while in the measurements of photo-induced electron transfer were made using a fairly high irradiation which gave $2 < \langle x \rangle_0 < 80$ (see Table 1-4). However, Rothenberger *et al* revealed also that k_r is almost constant if the $\langle x \rangle_0$ values are in a range from 0.85 to 300[27]. Since the fluorescence lifetime of each fraction was independent of the particle size as mentioned above, k_r at higher excitation intensity also seems to be independent of

the particle size. Further, Nosaka *et al* reported that k_r of Q-CdS did not vary for particles ranging from 4 to 2 nm[2c]. Considering these, $\tau_{1/2}$ must be proportional to α V(D) / $<x>_0$. Figure 1-11 shows that calculated $\tau_{1/2}$ is independent of the particle sizes, being independent of the fraction number, suggesting that the rate of carrier recombination is almost the same for all Q-CdS particles as long as my experimental conditions are concerned where relatively high irradiation was used. Then the electron concentration [e^-] in the Q-CdS particles may be regarded to be constant. The term [$MV^{2+}{}_{ad}$] in eq. 1-11, which is the concentration of adsorbed MV^{2+} per unit surface area of Q-CdS particles, is also constant irrespective of the particle size.

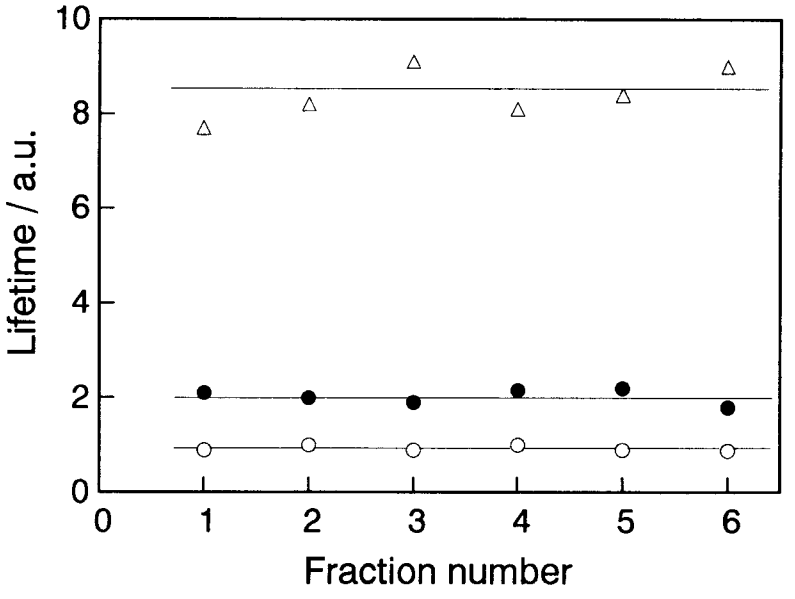

Figure 1-11 Size-dependence of lifetime (a.u.) of Q-CdS particles. Light intensity; (△) : 5 mW, (●) : 25 mW, (○): 50 mW.

Considering these, it may be said that the difference in the reduction rate, as shown in Figure 1-9, resulted from differences in the rate constant given by eq. 1-11. The reduction rate of MV^{2+} is enhanced with decreasing the particle size, due to a negative shift in the potential of the conduction band edge the degree being dependent on quantum size effects, and accordingly with decrease in the particle size the potential difference between the conduction band edge and the reduction

potentials of MV^{2+} is increased.

Referring to literature[28-30], the flat-band potentials of bulk CdS are rather scattered, but the most frequently reported values are about -0.9 V vs SCE, which is negative enough to reduce MV^{2+} whose redox potentials is -0.69 V vs. SCE. The magnitude of the negative shift of the conduction band edge due to the size quantization (ΔE_c) can be evaluated using theoretically derived relationships between the potential of the conduction band edge and particle size.[17] Since each fraction obtained by the gel electrophoreses contained Q-CdS particles of different sizes, I use the average $\Delta E_c(r)$ estimated by eq. 1-13.

$$\Delta E_c(r) = \sum_i \Delta E_c(r_i) F(r_i) \qquad (1\text{-}13)$$

where $F(r_i)$ is the frequency of the Q-CdS particles with radius r_i as shown in Figure 1-4.

If the rate of electron transfer to MV^{2+}, k_{et} , is controlled by the potential difference between the conduction band edge and MV^{2+}, an increase in the rate by the size quantization obeys the Tafel equation,

$$\log (k_{et} / k_{et}^0) = -(1-\alpha)\Delta E_c(r) / 0.059 \quad (\text{at } 25℃) \qquad (1\text{-}14)$$

where k_{et}^0 is the rate constant for electron transfer at the standard redox potential, and α is the transfer coefficient. Figure 1-12 shows Tafel-type plots of $\log r_{init}$ *vs* $\Delta E_c(r)$. A linear relationship is observed for the three different light intensities used. This suggests that the photoinduced reduction rate increases with the increase in potential difference caused by the size-quantization effects. The transfer coefficient determined from the slope is 0.30 ~ 0.33 and is independent of light intensity. Grätzel and Frank[1b] measured the rate of the photoinduced reduction of MV^{2+} on TiO_2 particles (d = *ca.* 20 nm) as a function of the solution pH. By changing the solution pH, the differences between the potential of the conduction

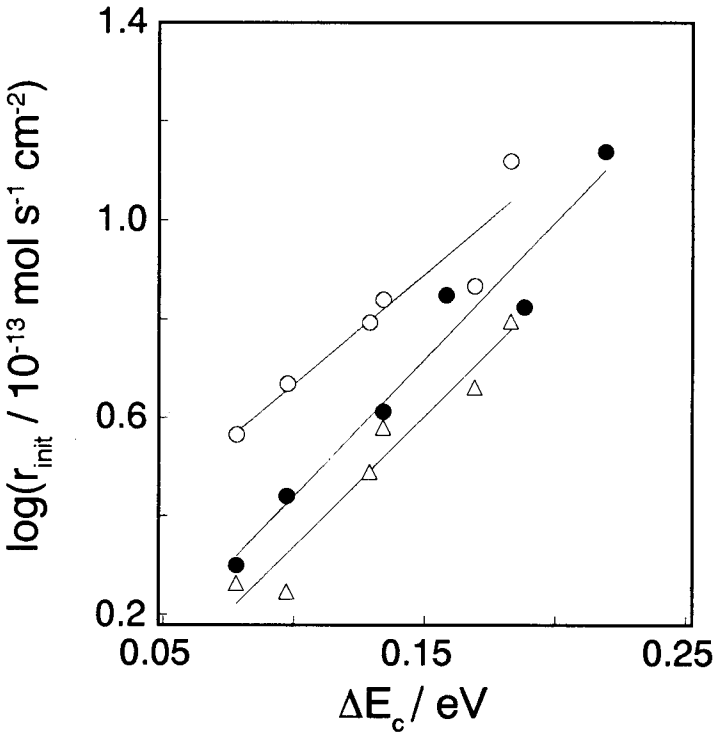

Figure 1-12 Plots of log r_{init} *vs* ΔE_c at 5 mW (△), 25 mW (●) and 50 mW (○) irradiation. Solid lines were least-square fits.

band edge of the TiO_2 particle and the redox potential of MV^{2+} was varied. By applying the Tafel relation in a similar manner, they obtained $\alpha = 0.52$. The smaller value of α obtained for the Q-CdS in the present work may be ascribed either to differences in the stabilizers or semiconductor materials used.

If it is assumed that the flat-band potential of bulk Q-CdS is -0.9 V vs SCE, the potential difference between the conduction band edge of Q-CdS particles and MV^{2+} (-0.69 V vs SCE[18]) or PVS^0 (-0.65 V vs SCE[31]) exceeds 200 mV. From viewpoints of electrochemical reactions of reversible systems, application of overpotentials as high as 200 mV or more usually results in a diffusion limited electrochemical reaction. However, the results given in Figure 1-5 evidence that the diffusion limited process was not operative in my experiments where pulsed laser irradiation was employed. Explanations of the activation controlled reaction may be done by evaluating the number of MV^{2+} involved in photoreduction with one shot irradiation. In the case of using one shot pulse of 25 mW, the experimentally determined quantum efficiency predicts that 3.2×10^{13} molecule $cm^{-3}$of MV^{2+} is

amount is negligibly small compared to the total amount of MV^{2+} originally present in the cell which is 6×10^{17} molecule cm^{-3}. However if the photoproduced MV^{+} on Q-CdS surface does not desorb, accumulation of adsorbed MV^{+} must cause its reoxidation by the valence band holes (eq. 1-8), giving a saturation tendency in the production of MV^{+}. Since the production of MV^{+} occurred linearly with illumination time for more than two hundreds irradiation with use of the laser pulse, the accumulation of MV^{+} on Q-CdS is unlikely. Accordingly, it is thought that MV^{+} produced by one shot irradiation desorbs during the interruption of irradiation (0.1 sec) to be replaced with new MV^{2+}.

In the present study, HMP was used as a stabilizer which is favorable for giving negative charges on the Q-CdS particles. The adsorption of MV^{2+} on the particles is assisted by such negative charges. In contrast, as already described above, photoreduction of PVS^{0} proceeded under diffusion control. Since PVS^{0} is electrically neutral, adsorption on Q-CdS particle surfaces is less likely.

1-4 References

1 (a) Duonghong, D; Ramsden, J; Grätzel, M *J. Am. Chem. Soc.* **1982**, *104*, 2977; (b) Grätzel, M.; Frank, A. J. *J. Phys. Chem.* **1982**, *86*, 2964; (c) Henglein, A. *Ber. Bunsenges. Phys. Chem.* **1982**, *86*, 241; (d) Bahnemann, D.; Henglein, A.; Lilie, J.; Spanhel, L. *J. Phys. Chem.* **1984**, *88*, 709; (e) Brown, G.T.; Darwent, J. R. J. Phys. Chem. **1984**, *88*, 4955; (f) Brown, G. T.; Darwent, J. R.; Fletcher, P. D. I. *J. Am. Chem. Soc.* **1985**,*107*, 6446; (g) Kölle, U.; Moser, J.; Grätzel, M. *Inorg. Chem.* **1985**, *24*, 2253; (h) Kamat, P. V. *Langmuir* **1985**, *1*, 608; (i) Darwent, J. R.; Lepre, A. *J. Chem. Soc., Faraday Trans. 2* **1986**, *82*, 2323; (j) Kamat, P.V.; Ebbesen, T.N.; Dimitrijevic, N.M.; Nozik, A.J. *Chem. Phys. Lett.* **1989**, *157*, 384; (k) Grabner, G.; Quint, R.M. *Langmuir*, **1991**, *7*, 1091; (l) Fitzmaurice, D.; Eschle, M.; Frei, H.; Moser, J. *J. Phys. Chem.* **1993**, *97*, 3806.

2 (a) Nedeljkovic, J. M.; Nenadovic, M. T.; Micic, O. I.; Nozik, A. J. *J. Phys. Chem.* **1986**, *90,* 12; (b) Watzke, H. J.; Fendler, J. H. *J. Phys. Chem.* **1987**, *91,* 854; (c) Nosaka, Y.; Ohta, N.; Miyama, H. *J. Phys. Chem.* **1990**, *94*, 3752; (d) Nosaka, Y. *J. Phys. Chem.* **1991**, *95*, 5054.

3 Rossetti, R.; Brus, L.E. *J. Phys. Chem.*, **1986**, *90*, 558.

4 Nosaka, Y.; Fox, M.A. *J. Phys. Chem.*, **1988**, *92*, 1893.

5 Inoue, H.; Torimoto, T.; Yoneyama, H. *Chem. Lett.*, **1990**, 1483.

6 Yoneyama, H. *Res. Chem. Intermed.*, **1991**, *15*, 101.

7 Nosaka, Y.; Fox, M.A. *Langmuir*, **1987**, *3*, 1147.

8 (a) Kamat, P.V.; Dimitrijevi , N.M.; Fessenden, R.W. *J. Phys. Chem.*, **1988**, *92*, 2324.

9 (a) Torimoto, T.; Uchida, H.; Sakata, T.; Mori, H.; Yoneyama, H. *J. Am. Chem. Soc.* **1993**, *115*, 1874; (b) Torimoto, T.; Sakata, T.; Mori, H.; Yoneyama, H. *J. Phys. Chem.* **1994**, *98,* 3036.

10 Ramsden, J.J.; Grätzel, M. *Chem. Phys. Lett.* **1986**, *132,* 267; Serpone, N.; Sharma, D.K.; Jamieson, M.A.; Grätzel, M.; Ramsdem, J.J. *Chem. Phys. Lett.* **1985**, *115*, 473.

11 Kamat, P.V.; Dimitrijevic, N.M. *J. Phys. Chem.* **1989**, *93*, 4259.

12 Eychmüller, A.; Katsikas, L.; Weller, H. *Langmuir* **1990**, *6*, 1605.

13 Katsikas, L.; Eychmüller, A.; Giersig, M.; Weller, H. *Chem. Phys. Lett.* **1990**, *172*, 201.

14 Eychmüller, A.; Hässelbarth, A.; Katsikas, L.; Weller, H. *Ber. Bunsenges. Phys. Chem.* **1991**, *95*, 79.

15 Spanhel, L.; Haase, M.; Weller, H.; Henglein, A. *J. Am. Chem. Soc.* **1987**, *109*, 5649.

16 (a) Henglein, A *Top. Curr. Chem.* **1988**, *143,* 113 ; (b) Henglein, A. *Chem. Rev.* **1989**, *89*, 1861.

17 Lippens, P.E.; Lanoo, M. *Phys. Rev. B* **1989**, *39*, 10935.

18 Watanabe, T.; Honda, K. *J. Phys. Chem.* **1982**, *86*, 2617.

19 Gutiérrez, M.; Henglein, A. *Ber. Bunsenges. Phys. Chem.* **1983**, *87*, 474.

20 Pourbaix, M. *Atlas of Electrochemical Equilibria in Aqueous Solution*, pp.414 (Pergamon Press, 1966).

21 Chestnoy, N.; Harris, T.D.; Hall, R.; Brus, L.E. *J. Phys. Chem.* **1986,** *90*, 3393.

22 O'Neil, M.; Marohn, J.; McLendon, G. *J. Phys. Chem.* **1990**, *94*, 4356.

23 Misawa, K.; Yao, H.; Hayashi, T.; Kobayashi, T. *Chem. Phys. Lett.*, **1991**, *183*, 113.

24 James, D. R.; Liu Y-S; Mayo, P. D.; Ware, W. R. *Chem. Phys. lett.* **1985**, *120*, 460.

25 (a) Kuczynski, J.; Thomas J. K. *J. Phys. Chem.* **1983**, 87, 5498 ; (b) Bahnemann, D. W. ; Kormann, C. ; Hoffmann, M.R. *J. Phys. Chem.* **1987**, 91, 3789 ; (c) Chrysochoos, J. *J. Phys. Chem.* **1992**, 96, 2868 ; (d) Hässelbarth, A. ; Eychmüller, A. ; Weller, H. *Chem. Phys. Lett.* **1993**, 203, 271.

26 Albery, W. J. *J. Chem. Soc.,Faraday Trans. 1* **1985**, *81*, 1999.

27 Rothenberger, G.; Moser, J.; Grätzel, M.; Serpone, N.; Sharma, D.K. *J. Am. Chem. Soc.* **1985**, *107*, 8054.

28 White, J. R.; Bard, A. J. *J . Phys. Chem.* **1985**, *89*, 1947.

29 Chang, A-C.; Fendler, J. H. *J. Phys. Chem.* **1989**, *93*, 2538.

30 (a) Watanabe, T.; Fujishima, A.; Honda, K. Chem. Lett. 1974, 807; (b) Ginley, D. S.; Butler, M. A. *J. Electrochem. Soc.* **1978**, *125*, 1968; (c) Dewitt, R.; Mesmaeker, A.K-D. *J. Electrochem. Soc.* **1983**, *130*, 1995; (d) Meissner, D.; Memming, R.; Kastening, B. *J. Phys. Chem.* **1988**, *92*, 3476; (e) Uchihara, T.; Matsumura, M.; Ono, J.; Tsubomura, H. *J. Phys. Chem.* **1990**, *94*, 415.

31 Willner, I. ; Yang, J.M. ; Laane, C. ; Otvos, J.W. ; Calvin, M. *J. Phys. Chem.* **1981**, *85*, 3277.

Chapter 2 Size Dependent Fluorescence Quenching of CdS Nanocrystals Caused by TiO_2 Colloids as a Potential-Variable Quencher

2-1 Introduction

The electron transfer on semiconductor nanocrystals has been one of major subjects in semiconductor electrochemistry.[1-14] It has been revealed that various factors influence the rate of electron transfers. For example, charged conditions of semiconductor surfaces [3,6,9a,9d,10a,13], the excitation intensity[10b-d], and particle size[5,7,10b,12] greatly affect the photoreduction rate of electron acceptors such as methyl viologen in solution.

From the view point of electrochemistry, the electron transfer rate must be affected by the potential difference between the semiconductor and the acceptors, as demonstrated for TiO_2-methylviologen $(MV^{2+})^2$ and CdS-MV^{2+} systems as described in chapter 1 where the rate of photo-reduction of MV^{2+} is enhanced by increasing the potential difference. In the case of TiO_2-MV^{2+} system, the potential difference was varied by changing the solution pH, while in the case of the latter, the potential difference was varied by changing the particle size of CdS in a size quantization regime. Similar experiments on the effect of the potential difference in the electron transfer rate can in principle be made by using a variety of electron acceptors having different redox potentials for one kind of semiconductor particles. However, the use of the different acceptors does not necessarily give clear information on the effect of the potential difference on the electron transfer rate because it is of no doubt that the reducibility of the electron acceptors is different among various electron acceptors.

It has been shown that the charge separation in a photoexcited semiconductor particles becomes efficient with addition of a suitable semiconductor particles of the other kind. The demonstration for this has been made for CdS-TiO_2[15a,d,f],

CdS-ZnO[15a], CdS-Ag_2S[15b], CdS-AgI[15d], Cd_3P_2-ZnO[15c] and CdS-HgS[15e]. For example, the photoreduction of MV^{2+} in CdS colloids enhanced to ca. 100 % of the quantum efficiency by addition of TiO_2 colloids at a high concentration.[15a] Similarly, fluorescence intensity of CdS colloids in acetonitrile is quenched by addition of TiO_2 and AgI colloids as a result of electron transfer from the former semiconductor to the latter. Comparative analysis of the fluorescence quenching behaviors based on the adsorption-desorption equilibrium for CdS-TiO_2 and CdS-AgI systems suggested that the rate of electron transfer is markedly influenced by the difference between the conduction band potentials of the two kinds of semiconductors.[15d] However, no report has been published on the size dependence of electron transfer behaviors in semiconductor coupling systems.

In this chapter, I report that the use of TiO_2 as a quencher for fluorescence at CdS nanocrystals (Q-CdS) of various sizes as a function of solution pH allows the determination of the size dependent conduction band potential of Q-CdS.

2-2 Experimental Section

2-2-1 Preparation of Size-separated CdS Colloids

Size separated CdS colloids which denoted Q-CdS were prepared as the same method shown in the previous chapter. The Q-CdS colloid solutions were optically transparent if their pHs were below pH 13.0, but the precipitation occurred at higher than pH 13.0 due probably to formation of $Cd(OH)_2$. The size distribution of Q-CdS particles was determined by observations by a transmission electron microscopy (TEM) (Hitachi, H-800).

2-2-2 Preparation of TiO_2 Colloids

The TiO_2 colloid was prepared following the method reported by Grätzel *et al.*[2a]

5 mL of isopropanol solution containing titanium tetraisopropoxide (1 g/L) was dropped slowly into 45 mL of acidic aqueous solution (pH 1.3, adjusted with $HClO_4$) under vigorous stirring and nitrogen bubbling. The absorption spectra of the resulting colloid was not remarkably changed at pHs higher than pH 8.5. The average diameter and the standard deviation of the TiO_2 colloids estimated from the TEM pictures were 3.0 nm and 0.8 nm, respectively.

2-2-3 Absorption and Fluorescence Measurements

Absorption spectra were measured using a Hewlett-Packard 8452A UV/Vis photodiode array spectrophotometer. Static fluorescence spectra were measured with a Hitachi F3010 fluorescence spectrometer. The absorbance of size separated Q-CdS colloids was adjusted to 0.04 at 360 nm using the aqueous solution containing 5 mM HMP and 5 mM $Cd(ClO_4)_2$. The resulting solution contained *ca.* 40 μM of CdS molecules, as evaluated using the absorption coefficient of 951 M^{-1} cm^{-1} at 360 nm which was determined for the Q-CdS colloids before size separation. The solution pH was adjusted using NaOH or $HClO_4$.

2-3 Results and Discussion

2-3-1 Optical Properties of Size-Separated Q-CdS

The absorption and fluorescence spectra of size separated Q-CdS colloids are shown in Figure 2-1a and Figure 2-1b, respectively. The average particle size, its standard deviation, the absorption threshold, and the wavelength at the fluorescence maximum of Q-CdS used in the present study are given in Table 2-1. As already known well, both absorption onset and fluorescence peak are blue-shifted with decreasing the particle diameter due to quantum size effects.[1,17]

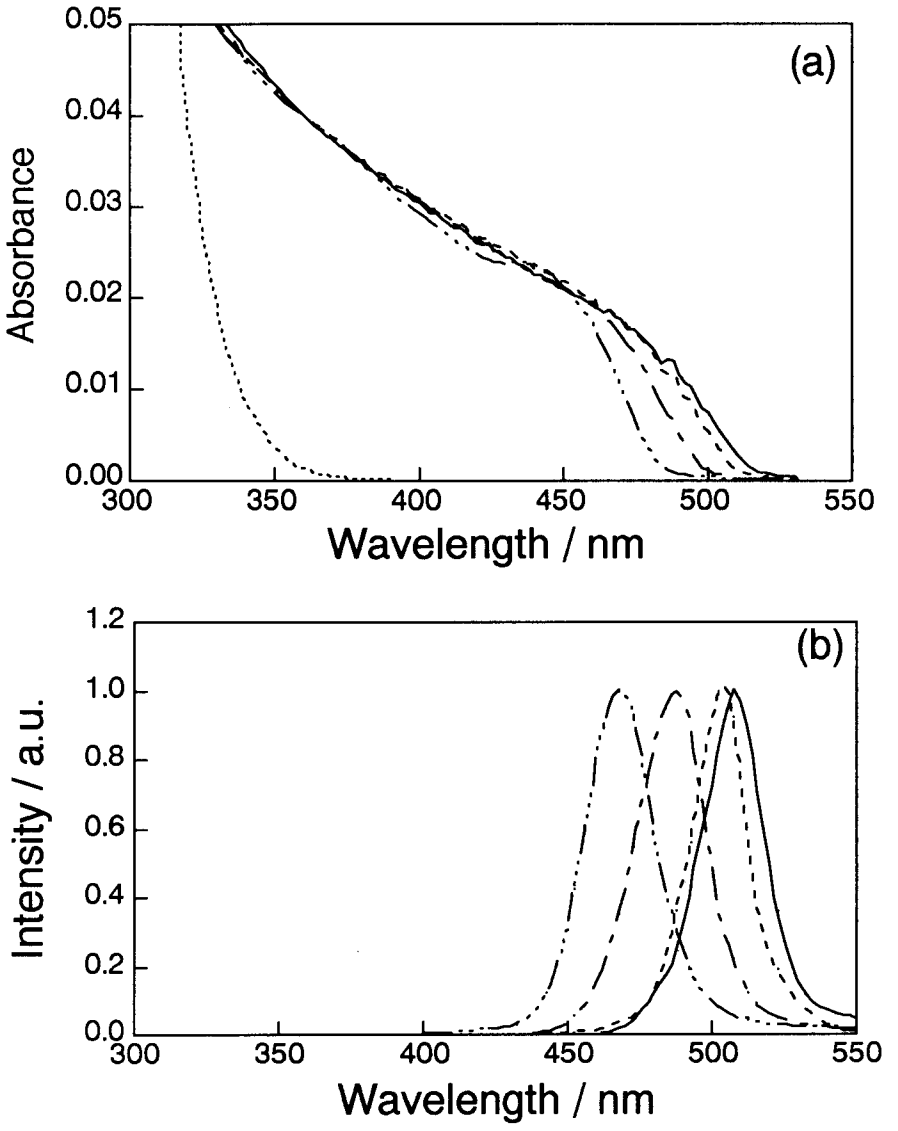

Figure 2-1 Absorption (a) and normalized fluorescence spectra (b) of Q-CdS of different sizes; (–····–) 3.2 nm, (– · –) 4.2 nm, (-----) 5.0 nm, (——) 6.2 nm. (·····) TiO_2 colloids. The concentration of Q-CdS was adjusted so as to give the absorbance of 0.04 at 360 nm in aqueous solution containing 5 mM HMP and 5 mM $Cd(ClO_4)_2$ having pH 11. Excitation: λ_{ex}=360 nm.

The fluorescence intensity (I') of Q-CdS increases with increasing the solution pH up to pH = 10 beyond which a saturation tendency appears, as shown in Figure 2-2. The fluorescence intensity is proportional to the fluorescence quantum yield (ϕ°_{em}), because the absorbance at the excitation wavelength was fixed to a constant value and the peak area of the fluorescence spectrum was nearly proportional to the peak intensity. Since the fluorescence quantum yield is correlated to the rate

Table 2-1 Physical and optical properties of Q-CdS.

d_{av} [a] /nm	σ_d [b] /nm	absorption onset /nm	fluorescence maximum /nm
6.2	1.4	514	505
5.0	1.3	509	502
4.2	0.8	496	485
3.2	0.6	481	466

a Average diameter of Q-CdS determined from TEM pictures.
b Standard deviation of the diameter determined from TEM pictures.

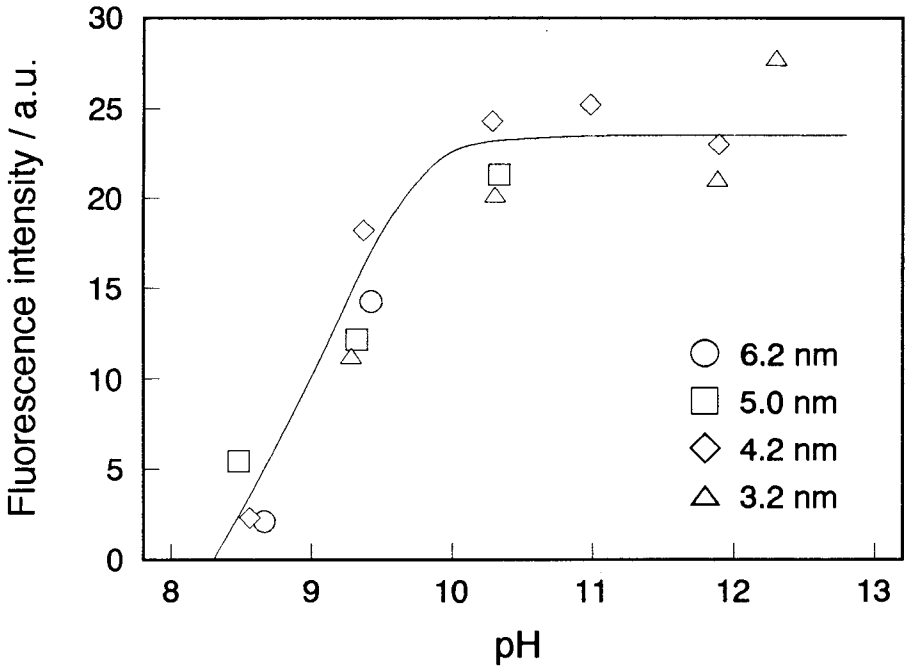

Figure 2-2 pH dependence of the fluorescence intensity of Q-CdS of various sizes, measured in aqueous solution containing 5 mM HMP and 5 mM $Cd(ClO_4)_2$.

constants of radiative (k_r) and non-radiative emission (k_{nr}) and the fluorescence lifetime τ, eq.2-1 holds.[18]

$$I^\circ \approx \phi^\circ_{em} = k_r / (k_r + k_{nr}) = k_r \tau \qquad (2\text{-}1)$$

Spanhel *et al.* previously explained the pH dependent change of ϕ° and τ in terms

of changes of the amount of $Cd(OH)_2$ at particle surfaces which blocks radiationless recombination sites.[17a] This explanation is in conformity with the fact that Cd^{2+} ions are more easily converted to $Cd(OH)_2$ at pH≥10. Judging from the finding that the fluorescence lifetime of Q-CdS at pH 11.0 obtained by a single-photon counting method was independent of the particle sizes as stated in chapter 1-3-3, the fluorescence lifetime of Q-CdS of different sizes may be regarded to be almost the same as long as the solution pH is not varied.

2-3-2 Quenching of Bandgap Fluorescence of Q-CdS Using TiO_2 Colloids

The fluorescence quenching of Q-CdS caused by addition of TiO_2 colloids occurs as a result of fast electron transfer from photoexcited Q-CdS to TiO_2.[15d,f] Certainly the fluorescence intensity of Q-CdS decreased with increasing the concentration of TiO_2, the degree being greater for smaller Q-CdS , as shown in Figure 2-3a. Furthermore, the fluorescence quenching was influenced by solution

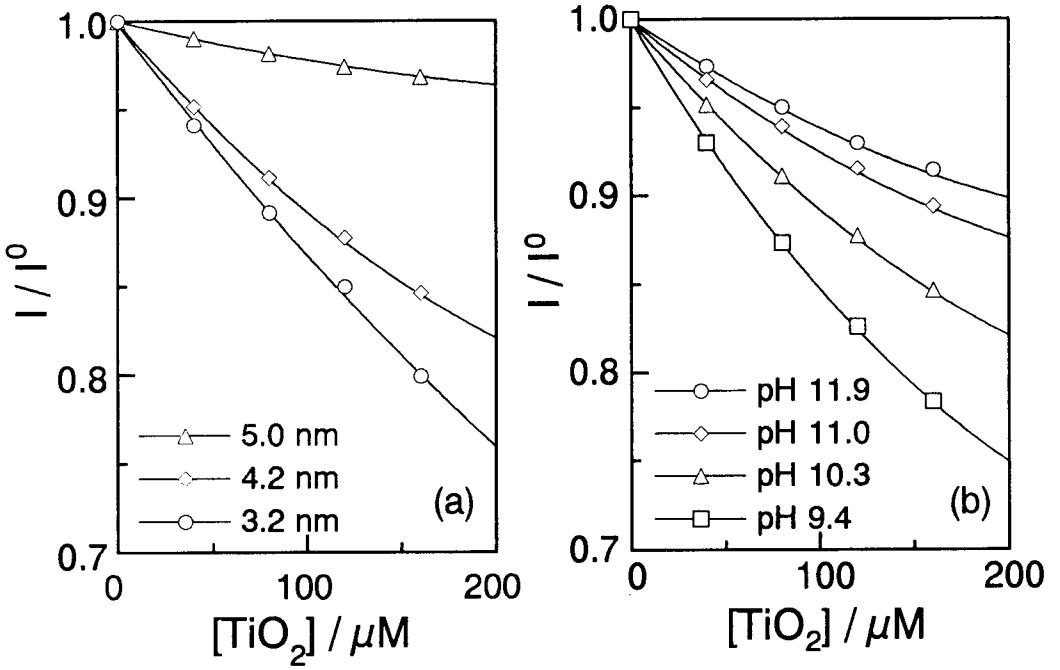

Figure 2-3 Decrease of fluorescence intensity of Q-CdS caused by addition of TiO_2 colloids of various concentrations. (a) size dependence obtained at pH = 10.3, (b) pH dependence at Q-CdS of 4.2 nm.

pH and was the greater for the lower solution pH (Figure 2-3b). In both cases, the enhancement of the efficiency of the quenching can be qualitatively explained in terms of increase in the potential difference of the conduction bands between Q-CdS and TiO_2 , which is denoted here as $\Delta E_{cb}(CdS\text{-}TiO_2)$. $\Delta E_{cb}(CdS\text{-}TiO_2)$ becomes great with decreasing the particle sizes of Q-CdS, because the potential of the conduction band of Q-CdS (E_{cb}(Q-CdS)) must be negatively shifted due to the quantum size effects. If E_{cb}(Q-CdS) is assumed to be independent of the solution pH, $\Delta E_{cb}(CdS\text{-}TiO_2)$ increases with decreasing the solution pH, because the flatband potential of TiO_2 ($E_{cb}(TiO_2)$) positively shifts with decreasing the pH. The TiO_2 particles used were 3.0 nm in the average size with the standard deviation of 0.8 nm, as described above. The bandgap of such small particles is greater than that of bulk TiO_2 due to size quantization effects. This contribution to the conduction band potential of TiO_2 is given by χ. The $E_{cb}(TiO_2)$ of the particles used in the present study is then given by

$$E_{cb}(TiO_2) = (-0.37 - 0.059\ pH) - \chi \quad (V\ vs.\ SCE) \qquad (2\text{-}2)$$

where (-0.37 - 0.059 pH) is the conduction band potential of TiO_2 colloids without size quantization.[2b] Though it is not easy to estimate χ , it was reported that a shift of the conduction band of TiO_2 of 2.0 nm was about 0.3 V[19]. Since the particle size of TiO_2 used in the present study was about 1 nm bigger, χ must be much smaller than 0.3 V.

2-3-3 Analysis of Quenching Process Based on Adsorption-Desorption Equilibrium Between CdS and TiO_2 Colloids

The quenching of Q-CdS with the addition of TiO_2 must occur only when Q-CdS adsorbs on TiO_2 particles.[15a,d] If the quenching process is dynamic and the rate of electron transfer is diffusion limited, the quenching rate constant of $\sim 10^{10}$

$M^{-1}s^{-1}$ would be expected.[18] The collision time (τ_{coll}) is then estimated to be 0.6 μs at the highest TiO_2 concentration using fluorescence quenching experiments (160 μM) from eq.2-3.

$$\tau_{coll} = \frac{1}{k_{et}[TiO_2]} \tag{2-3}$$

The estimated value is much larger than the fluorescence lifetime of Q-CdS of 45 ns at pH 11.0 for Q-CdS of various sizes as stated in chapter 1-3-3. The discrepancy suggests that the quenching process of Q-CdS is not dynamic. Kamat *et al* analyzed fluorescence quenching of Q-CdS by TiO_2 or AgI colloids based on association / dissociation equilibrium between the two.[15d] If the number of TiO_2 particles present in the solution is larger than that of Q-CdS, self-quenching of Q-CdS can be avoided, and then the method employed by Kamat *et al* is applicable to the present system. The following discussion leads to the conclusion that the number of TiO_2 particles was certainly greater than that of Q-CdS.

In the TiO_2 colloids used, 160 μM of TiO_2 was contained which was about 40 times as large as the concentration of CdS in the colloids used.(40 μM) By inserting these values to eq.2-4, the number of particles in the colloids (N_p) used was evaluated,

$$N_p = \frac{C_M \, M_W}{\rho \, V} \tag{2-4}$$

where M_w is the molecular weight of TiO_2 (or CdS), ρ is its density [g cm^{-3}], C_M is the molecular concentration of TiO_2 (or CdS) in the colloid used [M], N_p is the number of the semiconductor particles per dm^3 of colloids [particle dm^{-3}], V is the particle volume of individual particle [cm^3]. The number of Q-CdS particles estimated in this way is 2.0×10^{16} particle / dm^3, while that of Q-TiO_2 is 9.0×10^{17} particle / dm^3, the former being smaller than the latter. Then eq. 2-6 is valid for the

association dissociation equilibrium given by eq.2-5.[15d]

$$\text{Q-CdS} + \text{TiO}_2 \overset{K_{app}}{\rightleftharpoons} [\text{Q-CdS-TiO}_2] \tag{2-5}$$

$$\frac{1}{\phi^{\circ}_{em}-\phi_{em}(obsd)} = \frac{1}{\phi^{\circ}_{em}-\phi'_{em}} + \frac{1}{K_{app}(\phi^{\circ}_{em}-\phi'_{em})[TiO_2]} \tag{2-6}$$

where ϕ°_{em} and ϕ'_{em} is the fluorescence quantum yields of unassociated and associated CdS, respectively, $\phi_{em}(obsd)$ is the observed fluorescence quantum yields of Q-CdS in the presence of TiO_2, and K_{app} is the association constant. By multiplying both sides of eq.2-6 by ϕ°_{em}, eq.2-7 is obtained.

$$\frac{1}{1-\phi_r} = \frac{1}{1-\phi'_r} + \frac{1}{K_{app}(1-\phi'_r)[TiO_2]} \tag{2-7}$$

where ϕ_r is the relative fluorescence quantum yield defined by $\phi_{em}(obsd) / \phi^{\circ}_{em}$, and ϕ'_r is that defined by $\phi'_{em} / \phi^{\circ}_{em}$.

Since the fluorescence quantum yield is proportional to the fluorescence intensity as mentioned above, the left hand side of eq.2-7 may be replaced with $(1-I/I^{\circ})^{-1}$. As shown in figure 2-4, $(1-I/I^{\circ})^{-1}$ is certainly proportional to $[TiO_2]^{-1}$. The plots shown in Figure 2-4 allows the determination of ϕ'_r and K_{app} from intersection at the Y axis and the slope, respectively. The values of K_{app} and ϕ'_r obtained in this way under various solution pH for Q-CdS of various sizes are summarized in Table 2-2. The K_{app} values obtained here can be regarded to be almost the same for each particle size. The results seem reasonable because the fluorescent material and the quencher were fixed.

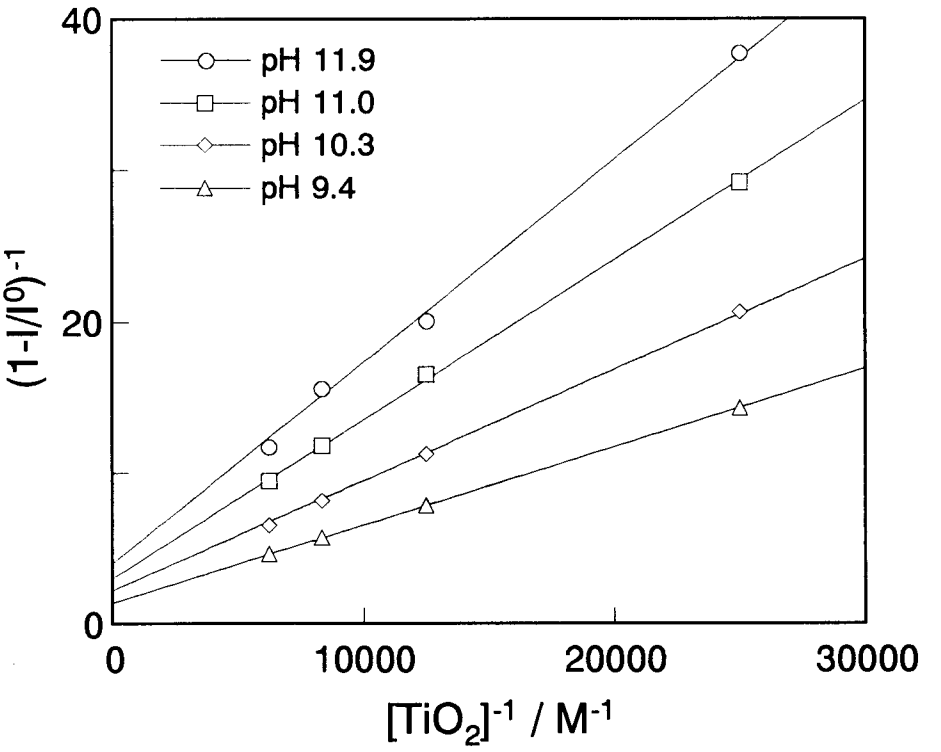

Figure 2-4 The plot of $(1-I/I^{\circ})^{-1}$ *vs*, $[TiO_2]^{-1}$ for Q-CdS of 4.2 nm. The data were taken from those given in Figure 2-3(b).

Table 2-2 K_{app} ($/10^3$) and ϕ'_r [a] obtained under various pHs at Q-CdS of different sizes.

diameter	pH= 8.5		pH=9.4		pH=10.3		pH=11.0		pH=11.9		pH=12.3	
/ nm	K_{app}	ϕ'_r	K_{app}	ϕ'_r	K_{app}	ϕ'_r	K_{app}	ϕ'_r	K_{app}	ϕ'_r	K_{app}	ϕ'_r
3.2			1.8	0.11	2.0	0.27			2.1	0.43	2.0	0.55
4.2	2.8	0.29	2.5	0.38	2.2	0.62	2.4	0.76				
5.0	2.8	0.45	3.6	0.57	2.6	0.94						
6.2	1.8	0.58	2.6	0.89								

a ϕ'_r is relative fluorescence quantum yields for associated CdS colloids, defined by $\phi'_{em} / \phi^{\circ}_{em}$

2-3-4 The Size Dependence of the Conduction Band Potential of Q-CdS

Figure 2-5 shows pH dependencies of $(1-\phi'_r)$, which are obtained from the results shown in Table 2-2. The $1-\phi'_r$ values are found to be affected by solution

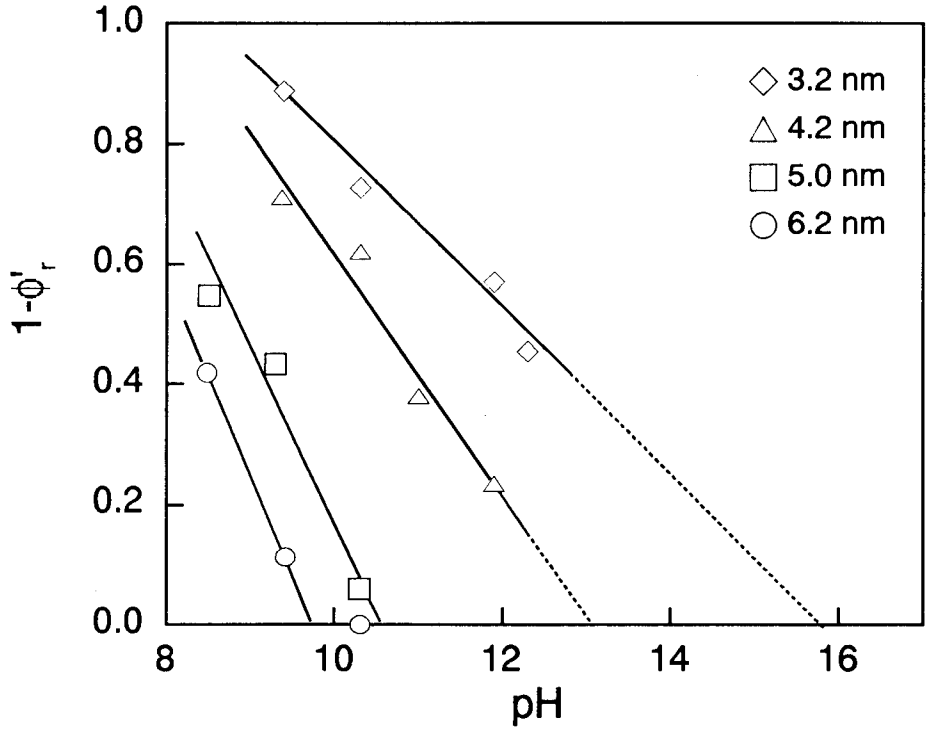

Figure 2-5 $(1-\phi'_r)$ as a function of pH for Q-CdS of various particle sizes. The data were taken from those given in Table 2-2.

pH, suggesting that the potential difference of the conduction bands between Q-CdS and TiO_2, ΔE_{cb}, plays an important role in the fluorescence quenching of Q-CdS as in the case of the fluorescence intensity (Figure 2-3). It seems likely that the rate of electron transfer from photoexcited Q-CdS to TiO_2 colloids (k_{et}) changes with changes in solution pH. Let the solution pH where $(1-\phi'_r)$ is equal to 0 be termed here as pH°. At that pH, ΔE_{cb} is approximated to zero, and E_{cb}(Q-CdS) is equal to $E_{cb}(TiO_2)$. The pH°values of Q-CdS of different sizes are estimated by extrapolating $(1-\phi'_r)$ *vs.* pH relations shown in Figure 2-5 to the abscissa. By applying the obtained pH°to eq.2-2, E_{cb}(Q-CdS) of various sizes can be evaluated. The obtained E_{cb}(Q-CdS) values contain a constant term of χ, and are -0.96 - χ V for 6.2 nm, -1.0 - χ V for 5.0 nm, -1.15 - χ V for 4.2 nm and -1.29 - χ V for 3.2 nm, as shown by dotted curves in Figure 2-6(a). The rate of the shift of E_{cb}(Q-CdS) with changes in the particle size obtained experimentally was much larger than that expected from tight binding approximation,[21] which is given by a solid curve in

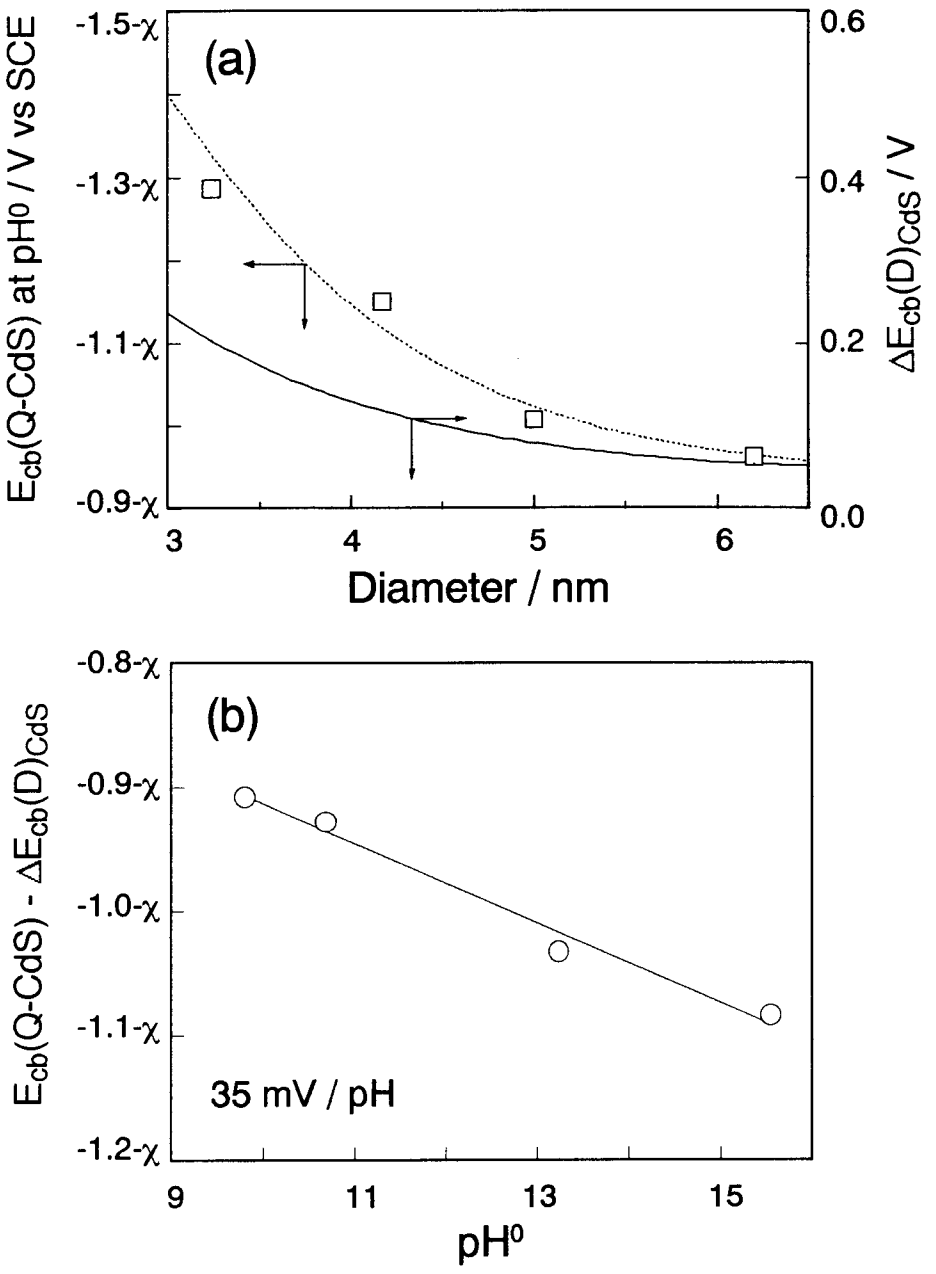

Figure 2-6 (a) Size dependence of the conduction band potential of Q-CdS at pH°, E_{cb}(Q-CdS) (dashed line) and the shift of conduction band due to the size quantization, predicted from tight-binding approximation, $\Delta E_{cb}(D)_{CdS}$ (full line). (b) E_{cb}(Q-CdS) - $\Delta E_{cb}(D)_{CdS}$ as a function of pH°.

Figure 2-6(a); 0.04 V for 6.2 nm, 0.072 V for 5.0 nm, 0.11 V for 4.2 nm, 0.19 V for 3.2 nm. It is then thought that the discrepancy may result from surface hydroxylation of Q-CdS, because as the plots given in Figure 2-5 show major data points of the plots were taken in solutions of pHs greater than pH 10 which is the threshold pH at which the surface hydroxylation of bulk CdS commences to take place.[22c] If it is

assumed that surface hydroxylation arises as a function of the solution pH for pH>10 and its contribution to the shift in the conduction band is given by $\Delta E_{cb}(pH)$ [V], the experimentally determined E_{cb}(Q-CdS) at pH°[V vs SCE] is given by

$$E_{cb}(Q\text{-}CdS) = E_{cb}(CdS)_{bulk} + \Delta E_{cb}(pH^\circ) + \Delta E_{cb}(D)_{CdS} \qquad (2\text{-}8)$$

where $\Delta E_{cb}(D)_{CdS}$ [V] is the shift of the conduction band potential due to the quantum size effect[21] of Q-CdS having the diameter D [nm], and $E_{cb}(CdS)_{bulk}$ [V vs SCE] is the conduction band potential of bulk CdS with no surface hydroxylation.

By deducting the contribution of the size quantization effect ($\Delta E_{cb}(D)_{CdS}$) from E_{cb}(Q-CdS) at pH°given in Figure 2-6(a), the results given in Figure 2-6(b) are obtained as a function of pH°. As this figure shows, (E_{cb}(Q-CdS) - $\Delta E_{cb}(D)_{CdS}$) have a linear dependence on pH°with the slope of about 35 mV / pH which is valid for bulk CdS having hydroxylated surface.[22c] Accordingly, the same surface hydroxylation seem to take place on Q-CdS, too. Referring to the results shown in Figure 2-5, the pH°of Q-CdS whose size is 6.2 nm is lower than pH 10, being lower than the threshold pH for the formation of surface hydroxylation. As shown in Figure 2-6(a), E_{cb}(Q-CdS) for the 6.2 nm diameter is -0.96 - χ V *vs.* SCE and $\Delta E_{cb}(D)_{CdS}$ is 0.04 V, respectively.

Then the conduction band potential of bulk CdS without surface hydroxylation is estimated to be -0.92 - χ V vs SCE by deducting the size quantization effects from -0.96 - χ V vs. SCE. The flat-band potential of bulk CdS having no surface hydroxylation is reportedly -0.92 V vs. SCE.[22] If the contribution of the size quantization effect χ were eventually null, the results obtained here are in agreements with the reported flat-band potential of bulk CdS. As already described above, the value of χ is not known though it must be much smaller than 0.3 V. If χ is not a negligible value, the existence of negatively charged HMP used as the stabilizer for Q-CdS might cause a negative shift of the conduction band potential of Q-CdS.

2-3-5 The Effect of the Potential Difference Between the Conduction Bands of Q-CdS and TiO_2 Colloids on Electron Transfer

The fluorescence quantum yields of the unassociated and associated Q-CdS with TiO_2 are given by eq.2-1 and eq.2-9, respectively.[15d]

$$\phi'_{em} = \frac{k_r}{k_r + k_{nr} + k_{et}} \tag{2-9}$$

where k_{et} is the rate constant of electron transfer.

If the radiative and nonradiative rate constant of the fluorescence quenching of Q-CdS is not affected by the presence of TiO_2, one can derive the following equation.

$$\frac{\phi^{\circ}_{em}}{\phi'_{em}} = \frac{1}{\phi'_r} = \frac{k_{et}}{k_r + k_{nr}} + 1 = \tau k_{et} + 1 \tag{2-10}$$

Rearrangements of eq. 2-10 gives[15d],

$$k_{et} = \left(\frac{1}{\phi'_r} - 1 \right) \frac{1}{\tau} \tag{2-11}$$

Recently, Zhang *et al* reported that the photogenerated electrons in Q-CdS are transferred to TiO_2 colloids within 2 ps.[15f] The electron transfer rate of $\sim 10^{12}$ s^{-1} or grater is then expected for the Q-CdS-TiO_2 system. If the rate constant of electron transfer for the present Q-CdS-TiO_2 system is estimated by eq.2-11, τ in eq.2-11 must then be in the order of 10^{-12} sec or the smaller. Unfortunately, I failed to measure the fluorescence decay of Q-CdS in a picosecond time domain due to instrumentation problems. However the results given in Figure 2-2, which shows

that the fluorescence intensity was not influenced by the particle size, may suggested that the fluorescence lifetime of Q-CdS in a picosecond time domain (τ of eq.2-11) is independent of the particle size. Zhang *et al* reported that photogenerated electrons are trapped on the surface of semiconductor nanocrystals such as Q-CdS and TiO_2 within 100 fs and that the rate of subsequent decay of trapped electrons is independent of the particle size.[20] Since τ in eq.2-11 may be regarded to be almost the same independent of the particle size as described here, k_{et} at Q-CdS of different sizes is obtained as a relative value with a variation of $(1/\phi'_r-1)$, which is given here as k_{et}'. Figure 2-7 shows k_{et}' obtained in this way using the data given in Table 2-2 as a function of $\Delta E_{cb}(CdS\text{-}TiO_2)$. If values of k_{et}' is given by their logarithm, then a Tafel relation is obtained, as included in Figure 2-7. The transfer coefficient α

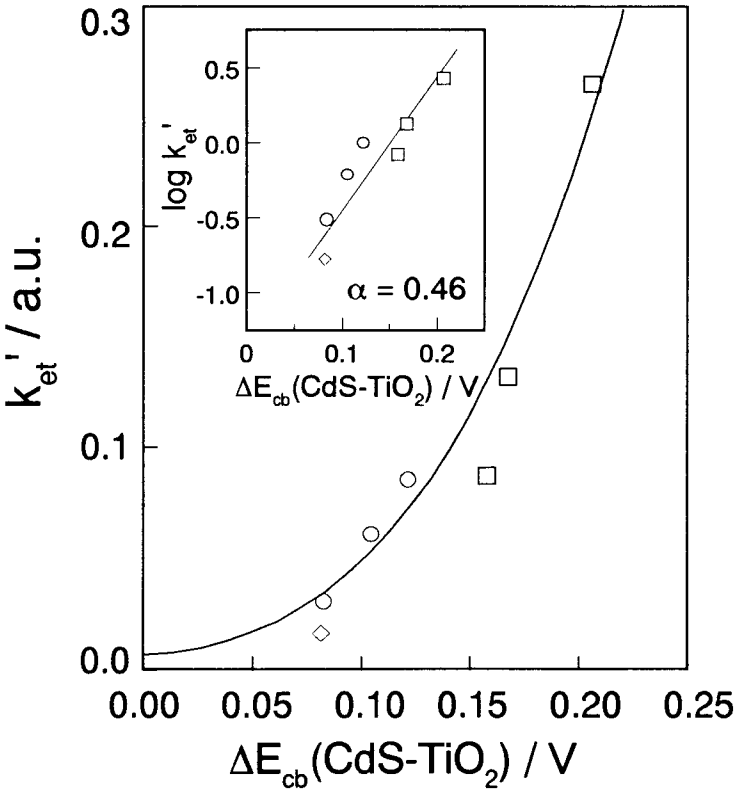

Figure 2-7 Plot of k_{et}' *vs.* potential difference between Q-CdS and TiO_2 colloids ($\Delta E_{cb}(CdS\text{-}TiO_2)$). Inset shows logarithmic plots of k_{et}' *vs.* $\Delta E_{cb}(CdS\text{-}TiO_2)$. k_{et}' was equal to $(\phi'_r{}^{-1}-1)$ and $\Delta E_{cb}(CdS\text{-}TiO_2)$ was evaluated from Figure 2-6.

obtained from the slope is 0.46, suggesting that the quenching process of Q-CdS caused by TiO_2 is indebted to electron transfer from Q-CdS to TiO_2 under activation control.

2-4 References

1 Recent reviews; (a) Henglein, A. *Chem. Rev.* **1989**, *89*, 1861; (b) Kamat, P.V. *Chem. Rev.* 1993, 93, 267; (c) Weller, H. *Angew. Chem. Int. Ed. Engl.* **1993**, *32*, 41.

2 (a) Duonghong, D.; Ramsden, J.; Grätzel, M. *J. Am. Chem. Soc.* **1982**, *104*, 2977; (b) Grätzel, M.; Frank, A.J. *J. Phys. Chem.* **1982**, *86*, 2964.

3 Bahnemann, D.; Henglein, A.; Spanhel, L. *Discuss. Faraday Soc.* **1984**, 78.

4 (a) Rossetti, R.; Nakahara, S.; Brus, L.E. *J. Chem. Phys.* **1983** *79*, 1086; (b) Rossetti, R.; Beck, S.M.; Brus, L.E. *J. Am. Chem. Soc.* **1984**, *106*, 980; (c) Rossetti, R.; Brus, L.E. *J. Phys. Chem.*, **1986**, *90*, 558.

5 (a) Brown, G.T.; Darwent, J.R. *J. Phys. Chem.* **1984**, *88*, 4955; (b) Brown, G.T.; Darwent, J.R.; Fletcher, P.D.I. *J. Am. Chem. Soc.* **1985**, *107*, 6446.

6 Kölle, U.; Moser, J.; Grätzel, M. *Inorg. Chem.* **1985**, *24*, 2253.

7 (a) Nedeljkovic, J.M.; Nenadovic, M.T.; Micic, O.I.; Nozik, A.J. *J. Phys. Chem.* **1986**, *90*, 12; (b) Watzke, H.J.; Fendler, J.H. *J. Phys. Chem.* **1987**, *91*, 854.

8 (a) Serpone, N.; Sharma, D.K.; Jamieson, M.A.; Grätzel, M.; Ramsden J.J. *Chem. Phys. Lett.* **1985**, *115*, 473; (b) Ramsden, J.J.; Grätzel, M. *Chem. Phys. Lett.* **1986**, *132*, 267.

9 (a) Kamat, P.V. *Langmuir* **1985**, 1, 608; (b) Kamat, P.V.; Dimitrijevic, N.M.; Fessenden, R.W. *J. Phys. Chem.* **1987**, *91*, 396; (c) Kamat, P.V.; Dimitrijevic, N.M.; Fessenden, R.W. *J. Phys. Chem.* **1988**, *92*, 2324; (d) Kamat, P.V.; Dimitrijevic, N.M. *J. Phys. Chem.* **1989**, *93* ,4259. (e) Kamat, P.V.; Ebbesen, T.W.; Dimitrijevic N.M. *Chem. Phys. Lett.* **1989**, *157*, 384. (f) Bedja, I.; Hotchandani, S.; Kamat, P.V. *J. Phys. Chem.* **1993**, *97*, 11064.

10 (a) Nosaka, Y.; Fox, M.A. *Langmuir* **1987**, *3*, 1147; (b) Nosaka, Y.; Fox, M.A. *J. Phys. Chem.* **1988**, *92*, 1893; (c) Nosaka, Y.; Ohta, N.; Miyama, H. *J. Phys. Chem.* **1990**, *94*, 3752; (d) Nosaka, Y. *J. Phys. Chem.* **1991**, *95*, 5054.

11 Moser, J.; Punchihewa, S.; Infelta, P.P.; Grätzel, M. *Langmuir* **1991**, *7*, 3012.

12 Rajh, T.; Micic, O.I.; Nozik, A.J. *J. Phys. Chem.* **1993**, *97*, 11999.

13 (a) Torimoto, T.; Uchida, H.; Sakata, T.; Mori, H.; Yoneyama, H. *J. Am. Chem. Soc.* **1993**, *115*, 1874; (b) Torimoto, T.; Sakata, T.; Mori, H.; Yoneyama, H. *J. Phys. Chem.* **1994**, *98*, 3036.

14 (a) Rossetti, R.; Brus, L. *J. Phys. Chem.* **1982**, *86*, 4470; (b) Kuczynski J.; Thomas, J.K. *J. Phys. Chem.* **1983**, *87*, 5498; (c) Weller, H.; Koch, U.; Gutiérrez, M.; Henglein, A. *Ber. Bunsen-Ges. Phys. Chem.* **1984**, *88*, 649; (d) Ramsden, J.J.; Grätzel, M. *J. Chem. Soc., Faraday Trans. 1* **1984**, *80*, 919; (e) Bahnemann, D.W.; Kormann, C.; Hoffmann, M.R. *J. Phys. Chem.* **1987**, *91*, 3789. (f) Chandler, R.R.; Coffer, J.L. *J. Phys. chem.* **1991**, *95*, 4; (g) Chandler, R.R.; Coffer, J.L.; Atherton, S.J.; Snowden, P.T. *J. Phys. Chem.* **1992**, *96*, 2713; (h) Chrysochoos, J. *J. Phys. Chem.* **1992**, *96*, 2868; (i) Chandler, R.R.; Coffer, J.L. *J. Phys. Chem.* **1993**, 97, 9767; (j) Hässelbarth, A.; Eychmüller, A.; Weller, H. *Chem. Phys. Lett.* **1993**, *203*, 271.

15 (a) Spanhel, L.; Weller, H.; Henglein, A. *J. Am. Chem. Soc.* **1987**, *109*, 6632; (b) Spanhel, L.; Weller, H.; Fojtik, A.; Henglein, A. *Ber. Bunsen-Ges. Phs. Chem.* **1987**, *91*, 88; (c) Spanhel, L; Henglein, A.; Weller, H. *Ber. Bunsen-Ges. Phs. Chem.* **1987**, *91*, 1359; (d) Gopidas, K.R.; Bohorquez, M.; Kamat, P.V. *J. Phys. Chem.* **1990**, *94*, 6435; (e) Hässelbarth, A.; Eychmüller, A.; Eichberger, R.; Giersig, M.; Mews, A.; Weller, H. *J. Phys. Chem.* **1993**, *97*, 5333; (f) Evans, J.E.; Springer, K.W.; Zhang, J.Z. *J. Chem. Phys.* **1994**, *101*, 6222.

16 Eychmüller, A.; Katiskas, L.; Weller, H. *Langmuir* **1990**, *6*, 1605.

17 (a) Spanhel, L.; Hasse, M.; Weller, H.; Henglein, A. *J. Am. Chem. Soc.* **1987**, *109*, 5649; (b) Eychmüller, A.; Hässelbarth, A.; Katsikas, L.; Weller, H. *Ber.*

Bunsen-Ges. Phys. Chem. **1991**, *95*, 79; (c) Hässelbarth, A.; Eychmüller, A.; Weller, H. *Chem. Phys. Lett.* **1993**, *203*, 271

18 Lakowicz, J.R. *Principles of Fluorescence Spectroscopy*; Plenum Press: New York, 1983.

19 Miyoshi, H.; Nippa S.; Uchida, H.; Mori, H. and Yoneyama H. *Bull. Chem. Soc. Jpn.* **1990**, *63*, 3380.

20 (a) Zhang, J.Z.; O'Neil, R.H.; Roberti, T.W. *Appl. Phys. Lett.* **1994**, *64*, 1989; (b) Zhang, J.Z.; O'Neil, R.H.; Roberti, T.W. *J. Phys. Chem.* **1994**, *98*, 3859.

21 Lippens, P.E.; Lanoo, M. *Phys. Rev. B* **1989**, *39*, 10935.

22 (a) Watanabe, T.; Fujishima, A.; Honda, K. *Chem. Lett.* **1974**, 807; (b) Ginley, D.S.; Butler, M.A. *J. Electrochem. Soc.* **1978**, *125*, 1968; (c) Dewitt, R.;Mesmaeker, A.K-D. *J. Electrochem. Soc.* **1983**, *130*, 1995; (d) Uchihara, T.; Matsumura, M.; Ono, J.; Tsubomura, H. *J. Phys. Chem.* **1990**, *94*, 415.

Chapter 3 Narrowing Size Distribution of CdS Nanocrystals by Size Selective Photocorrosion

3-1 Introduction

Semiconductor nanocrystals (Q-particles) exhibit unique properties which are different from those of bulk crystals due to quantum size effects.[1] Since chemical and physical properties of Q-particles depend on their size, it is desired to prepare monodispersed Q-particles to investigate the properties as a function of their size. So far, various techniques have been employed to achieve this. They are roughly classified into three categories.

The first approach is to use a limit space of nm dimensions as a reaction zone for Q-particle synthesis. For this purpose, solid materials having a limited space is useful. The cavities of zeolites[2], and interlayer spaces of clays[3] are useful as the reaction zone where Q-particles are synthesized. Inverse micells have often been used with the same objectives[4]. The use of inverse micells is useful for preparation of Q-particles but prepared Q-particles have usually a size distribution more or less.

The second approach is concerned with preparation under rigid control. The composition and concentration of reagents used for synthesis of Q-particles, and temperature of the preparation bath are carefully controlled[5].

The third approach is concerned with post treatments of prepared Q-particles prepared by the second approach. Chemically synthesized Q-particles are subjected to chromatography[6], capillary electrophoresis[7], gel electrophoresis as described in chapter 1 and sedimentation precipitation to result in size dependent separation.[8,9]

These three techniques are useful in narrowing the size of Q-particles from the original one, but the obtained Q-particles usually have a size distribution more or less. Among the post treatments described above, the last technique gave nearly monodispersed Q-CdS and Q-CdSe whose standard deviations approximately

± 5% of the mean diameter of the particles[8]. However, the sedimentation / precipitation method requires surface modification of Q-particles with organic modifiers such as thiol compounds, which may limit utility of this techniques.

In this chapter, a novel and easy preparation of as-prepared Q-CdS colloidal particles is described in which the size selective photocorrosion is used. It is well established that chalcogenide semiconductor particles are photodegradeded in aqueous solution if light irradiation with energy high enough to cause bandgap excitation is made[10]. Since the bandgap of Q-CdS is different depending on their size, and the smaller the particle size, the greater the bandgap, photoexcitation of the larger Q-CdS is easily done by irradiation with light of the longer wavelengths where the smaller Q-CdS is not photoexcited and then not photocorroded. In the present chapter, this idea has been successfully utilized for preparation of Q-CdS of vary narrow size distribution.

3-2 Experimental Section

CdS nanocrystals, which are denoted in this chapter as Q-CdS, were prepared as described in chapter 1. The average diameter and standard deviation of the Q-CdS was 42 Å and 19 Å, respectively as determined by observations of transmission electron micrographs (TEM) obtained by a Hitachi H-9000 transmission electron microscope operated at 300 keV. The prepared Q-CdS had a zinc-blende structure.

A 500 W Xe lamp was used as a light source and monochromatic light of desired wavelength was obtained using interference filters. The peak width at half height of the monochromatic light was about 10 nm. The monochromatic light was irradiated onto 2.0×10^{-3} dm^{-3} of air-saturated Q-CdS colloid in a quartz cell (1 cm × 1cm × 4 cm). Absorption spectra of the colloid was measured intermittently during the course of irradiation using a photodiode-array spectrophotometer (Hewlett-Packard, HP8452), and the irradiation with the monochromatic light was continued until no change in absorption spectra was observed. It usually took

several hours to achieve this.

The concentration of sulfate ions produced by the photocorrosion of Q-CdS was determined using a high performance liquid chromatography (Tosoh, CCPE) equipped with anion exchange column (Tosoh, TSKgel IC-Anion-PW) and detector (Tosoh, CM-8010). Borate buffer (1.3 mM, pH = 9.1) was used as an eluent at a flow rate of 1.0 ml/min.

When the particle size of the photocorroded Q-CdS was not determined directly by TEM pictures, it was estimated by applying the wavelength of the first exciton peak or shoulder of the absorption spectra of Q-CdS to the two theoretically derived relationship between particle size and the bandgap energy . One is the tight-binding approximation derived by Lippens *et al*[11] which is valid for Q-CdS as described in Chapter 1. However they calculated only the bandgap which corresponds to the lowest transition energy of the electron and hole in semiconductor nanocrystals, $1S_h$-$1S_e$. Since higher transition energies such as $2S_h$-$2S_e$ or $3S_h$-$3S_e$ cannot be obtained by this method, another method is adopted to calculate the photoexcitation to higher states using the finite depth potential well model derived by Nosaka.[12] In the calculation the effective mass of an electron and a hole of Q-CdS of 0.18 and 0.53, respectively, dielectric constant of 5.6, the depth of potential well of 3.6 (eV), and the bandgap of 2.4 (eV) were used. The lowest transition energy (bandgap) at Q-CdS of a desired diameter obtained by the finite depth potential well model was in good accordance with that obtained by the tight-binding methods.[11] Since these two methods cannot be simply solved analytically, no analytical formula was obtained. The various optical transition energy of the Q-CdS particles can be obtained by numerical calculations using a personal computer or the data in reported the references.[11,12]

3-3 Results and Discussion

3-3-1 Photocorrosion of Q-CdS by White Light

The photocorrosion of CdS has been well-established, and confirmed with the previous study, too. Irradiation with a 500 W Xe lamp to 1.8×10^{-4} mol dm^{-3} Q-CdS colloid (pH 6.0) in the presence of dissolved air caused complete disappearance of absorption spectra of Q-CdS after irradiation for a few hour, and the theoretically predicted amount of SO_4^{2-} ions (1.8×10^{-4} mol dm^{-3}) was produced. The solution pH was unchanged with photocorrosion of Q-CdS, and then the reaction scheme given by eq. 3-1~3-3 seems valid, as already reported previously.[13]

anodic reaction

$$CdS + 4h^+ + 2H_2O + O_2 \longrightarrow Cd^{2+} + SO_4^{2-} + 4H^+ \quad (3\text{-}1)$$

cathodic reaction

$$O_2 + 4e^- + 2H^+ \longrightarrow 2OH^- \quad (3\text{-}2)$$

overall stoichiometry for the photoprocess

$$CdS + 2O_2 \longrightarrow Cd^{2+} + SO_4^{2-} \quad (3\text{-}3)$$

3-3-2 Photocorrosion of Q-CdS by Monochromatic Light

When photoirradiation was initiated using monochromatic light of 500 nm for original Q-CdS colloid, its absorption spectrum was gradually changed and after a few hours of irradiation, a stable absorption spectrum (b) of Figure 3-1 was obtained. Subsequent irradiation at 480 nm gave a steady spectrum (c), and finally a spectrum (e) was obtained by irradiation at 430 nm. The results obtained here suggest that Q-CdS particles are photocorroded to the extent that gives the absorption onset equal to the wavelength of the irradiated photons. However the absorbance shown in Figure 3-1, the number of Q-CdS nanocrystals seems to have

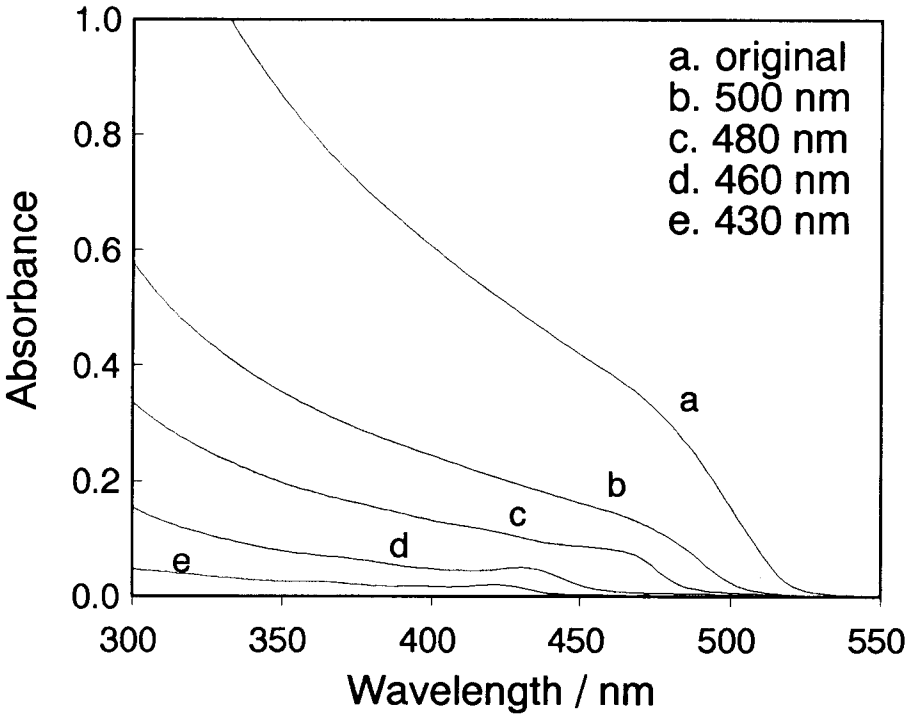

Figure 3-1 Absorption spectra of Q-CdS before and after irradiation with monochromatic light. (a) before irradiation, (b) 500 nm, (c) 480 nm, (d) 460 nm, (e) 430 nm.

decreased with decreasing the wavelength for irradiation. Presumably, HMP working as a stabilizing agent desorbs from Q-CdS surfaces in the photocorrosion, resulting in aggregation of Q-CdS particles which were then photocorroded further. The change of the total particle number caused by size selective photocorrosion will discussed later based on the results of qualitative analysis of the SO_4^{2-} ions contained in the solution after a series of irradiations by ion-chromatography.

Figure 3-2 shows normalized absorption spectra for the data in Figure 3-1, obtained by dividing the absorbance at each wavelength by that at the first exciton peak or shoulder. Structured absorption spectra are emerged with the decreasing the wavelength of monochromatic light used. This is especially prominent for the case of 430 nm, for which three exciton peaks are seen. The development of clear exciton peaks is indicative of monodispersive distribution of Q-CdS prepared.[8,9]

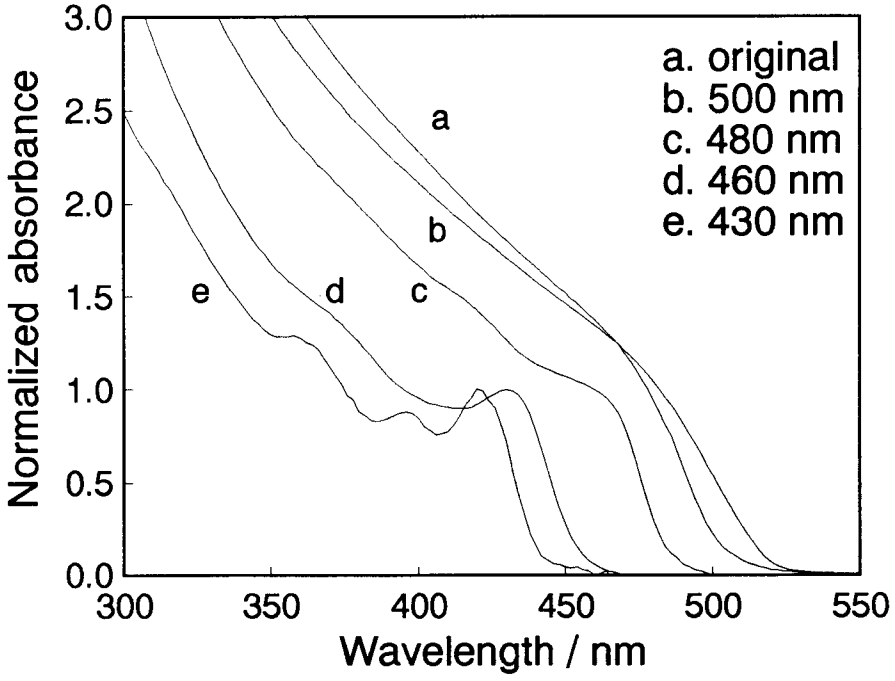

Figure 3-2 Normalized absorption spectra of Figure 3-1, obtained by dividing the absorbance of each wavelength by that of the first exciton peak or shoulder.

Figure 3-3 shows the size distributions of Q-CdS obtained from the results of transmission electron micrography (TEM) at three different stages of the irradiation. The electron diffraction patterns simultaneously obtained with TEM revealed that Q-CdS had a zinc-blende structure. It is seen that the larger particles of Q-CdS colloids were removed by the irradiation with the monochromatic light, and the standard deviation of the size distribution decreased with decreasing the wavelength of monochromatic light used. As shown in Table 3-1, the average diameters obtained by TEM observation (D_{TEM}) are in good accordance with the theoretically estimated diameters (D_{calc}) which were obtained by applying the exciton peak or shoulder of Q-CdS spectra to the reported energy gap *vs.* particle diameter relation.[11] The particle diameters evaluated from the absorption onset instead of the exciton peak or the shoulder are given in Table 3-1 as D_{onset} and also in Figure 3-3 with filled bars. Since the absorption onset of Q-CdS is determined by the largest particles present in the colloid with an amount not to be negligible,

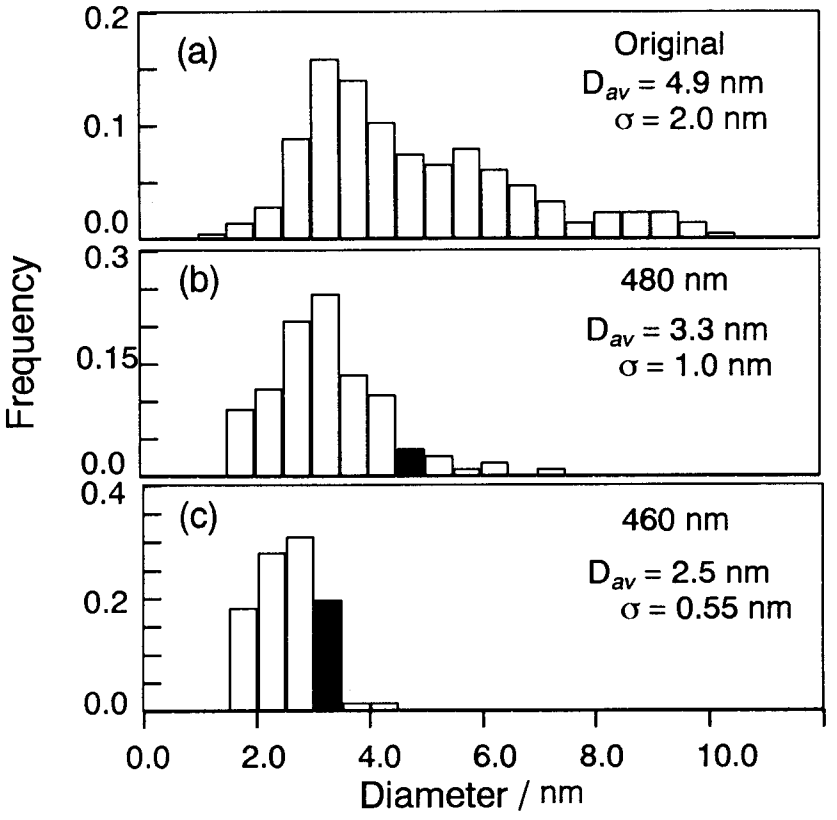

Figure 3-3 Size distribution of Q-CdS particles obtained by TEM pictures. The average diameter and its standard deviation are denoted by D_{av} and σ, respectively. (a) before irradiation, (b) and (c) after irradiation with monochromatic light of 480 nm and 460 nm, respectively. The diameter theoretically derived from the absorption onset is given by filled bars.

the evaluated D_{onset} seems to be reasonable.

The standard deviation and the average diameter for the 430 nm irradiation were not determined because the amount of Q-CdS particles obtained in that case was too small to be applied to TEM observations. However, considering the fact that the difference between D_{onset} and D_{calc} was nearly equal to the standard deviation (σ) for the cases of irradiation at 480 and 460 nm, CdS particles prepared with irradiation at 430 nm may have a distribution of their size roughly equal to the difference between D_{onset} and D_{calc}, which is 0.2 nm (= 2.8 - 2.6). Since the value of 0.2 nm is smaller than the lattice distance of CdS (0.25 nm), it is then concluded that a highly monodispersed distribution must have been achieved by irradiation at 430 nm as suggested by the appearance of clear exciton peaks, as already described.

Table 3-1 Size parameters of the photoetched Q-CdS obtained by TEM observations and using the theoretically derived relationship by Lippens *et al.*[11]

sample	E_g[a] /eV	D_{calc}[b] /nm	D_{TEM}[c] /nm	σ[d] /nm	λ_{onset}[e] /nm	E_{onset}[f] /eV	D_{onset}[g] /nm
original	2.57	4.6	4.9	2.0	520	2.38	>8
500 nm	2.59	4.2	n.d.[h]	n.d.[h]	503	2.47	5.8
480 nm	2.65	3.8	3.3	1.0	486	2.55	4.7
460 nm	2.84	2.8	2.5	0.55	454	2.73	3.3
430 nm	2.92	2.6	-	-	438	2.83	2.8

[a] Exciton energy estimated from the first exciton peak or shoulder given in Figure 3-1. [b] Particle diameter determined by applying E_g to the reported energy gap *vs.* particle diameter relation.[11] [c] Average diameter determined from TEM pictures. [d] Standard deviation. [e] Absorption onset. [f] Photon energy at λ_{onset}. [g] Particle diameter determined by applying E_{onset} to reported energy gap *vs.* particle diameter relation.[11] [h] not determined.

3-3-3 Precise Size Control of Monodispersed Q-CdS

As described above, the well structured absorption spectra can be obtained by the monochromatic light irradiation. In this section, the monochromatic light irradiation was applied to monodispersed Q-CdS particles of a large size to prepare monodispersed smaller Q-CdS particles. Figure 3-4 shows the steady-state absorption spectra of Q-CdS colloids obtained after irradiation with monochromatic light of the wavelength shown in the figure. The well structured spectra of Q-CdS begun to emerge at 460 nm monochromatic light irradiation. These peaks might be assigned to the various discrete transition energy of monodispersed semiconductor nanocrystals as schematically shown in Figure 3-5.[12] The white arrow in Figure 3-4 shows the $1P_h$-$1P_e$ transition energy which is higher than that of $1S_h$-$1S_e$ given by black arrows. The $1P_h$-$1P_e$ transition was calculated as follows. At first, the particle diameter was estimated by the first exciton peak with use of the finite depth potential well model as stated in experimental section. Then the second higher exciton energy ($1P_h$-$1P_e$) for the same diameter can be obtained by the same model. Another peaks which are seen between the first and the second exciton

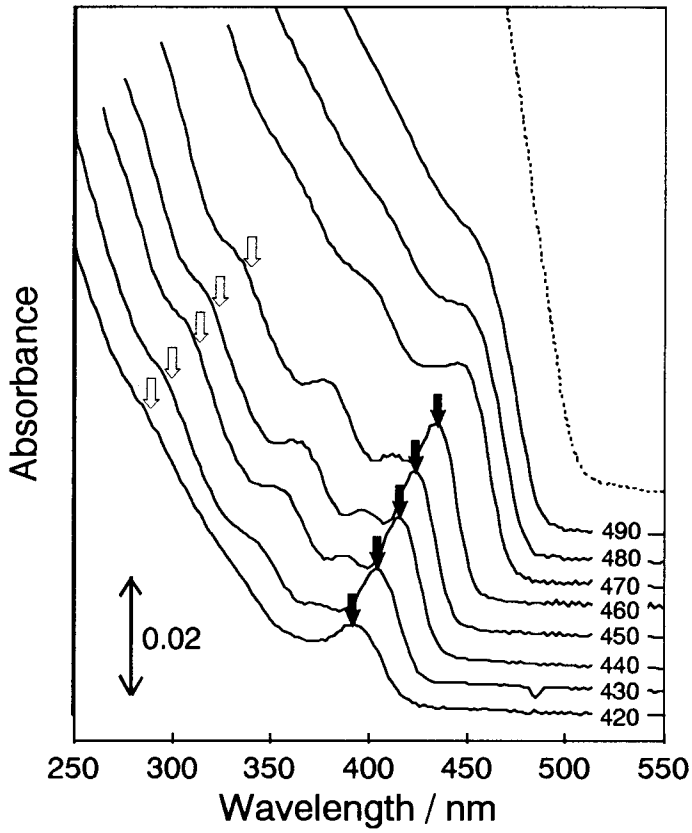

Figure 3-4 Steady-state absorption spectra of Q-CdS colloids obtained after irradiation with monochromatic light of the wavelength shown in the figure.(Black arrow) $1S_h$-$1S_e$ transition, (White arrow) $1P_h$-$1P_e$ transition.

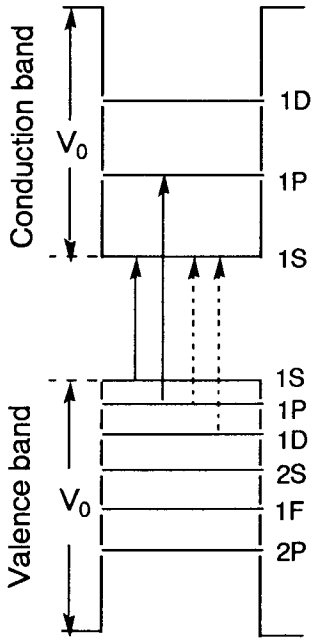

Figure 3-5 Schematic illustration of discrete bands derived from the finite depth potential well model.[12] V_0 is 3.6 eV of the potential well. (Full line) allowed transition, (Dotted line) forbidden transition.

peak might be assigned to the forbidden transition such as $1P_h$-$1S_e$ or $1D_h$-$1S_e$. Unfortunately, the calculation for these forbidden transitions could not been carried out because the coulomb interaction of an electron and a hole for the forbidden transition is not known. Anyway the good agreement between the calculated $1P_h$-$1P_e$ transition energy and the experimental results was obtained in the first time in the present study. The agreement shows that the finite depth potential well model is valid for the estimation of higher transitions than the $1S_h$-$1S_e$ (bandgap) of Q-CdS and the appearance of various exciton peaks must be indebted to highly monodispersed Q-CdS. If size distribution is not monodispersive, the exciton peak might disappear because of the overlapping of the exciton peaks arising from various particle sizes as shown in Figure 3-1 and Figure 3-3. Furthermore these findings shows that the precise control of particle size can be easily achieved by the selection of the appropriate wavelength of the monochromatic light.

3-3-4 Estimation of the Total Number of Q-CdS Particles by Quantitative Analysis of Sulfate Ions

The absorbance of the original Q-CdS colloid was decreased by irradiation with monochromatic light as shown in Figure 3-1. If photocorrosion was completed in such extent that the particles become so small as not to allow absorption of irradiated photons the total particle number of Q-CdS must be unchanged before and after the monochromatic irradiation. However this was not the case as described above. In order to estimate the change of the total number of the Q-CdS particles under the photocorrosion process, the amount of photodissolved Q-CdS was estimated as a function of excitation wavelength based on the amount of sulfate ions produced by photocorrosion which was determined using ion chromatography. In this experiments, 0.1 mM of methyl viologen was added to the Q-CdS solutions to enhance the rate of the dissolution of Q-CdS for rapid analysis of the estimation of sulfate ion. As previously reported[10], the rate of photocorrosion of Q-CdS or

Q-ZnS were dramatically enhanced by the addition of methylviologen to Q-CdS colloids. In that case, photogenerated electrons are quickly scavenged by the methylviologen, resulting in decrease in recombination of photogenerated electrons and holes in the semiconductor particles, and then photogenerated holes are effectively involved in photoanodic dissolution of Q-CdS (eq. 3-3).

As shown in Figure 3-6, the amount of sulfate ions determined after completion of photocorrosion increased with decreasing the irradiation wavelength, and the final amount of sulfate ions obtained when complete decomposition was achieved with irradiation at 420 nm monochromatic light (1.8×10^{-4} mol dm^{-3}) was in agreement with that obtained by irradiation with white light. Then total volume of Q-CdS particles present in the original colloids is given by eq. 3-4,

$$V_0 = [1.8 \times 10^{-4}] \times M_{CdS} / \rho = 5.4 \times 10^{-3} \ (cm^3) \qquad (3\text{-}4)$$

where 1.8×10^{-4} (mol dm^{-3}) is the concentration of original Q-CdS colloids, M_{CdS}

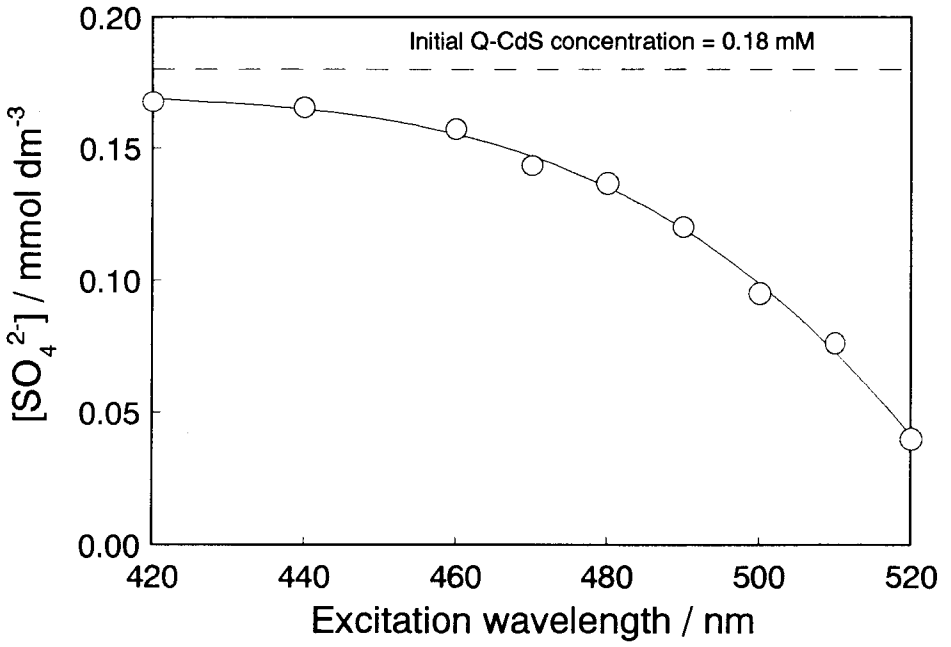

Figure 3-6 The amount of the sulfate ions produced by irradiation of Q-CdS colloid with monochromatic light given in the figure as the excitation wavelength.

is the molecular weight of CdS (144 g mol^{-1}), ρ is the density of bulk CdS (=4.82 g cm^{-3}). The total number of Q-CdS can be also calculated by using the relationship between V_0 and the size distribution of Q-CdS as shown in Table 3-2.

$$V_0 = N \sum_i f_i v_i \qquad (3\text{-}5)$$

where N is the total number of Q-CdS , and f_i and v_i are the frequency and volume of the fraction *i* in size distribution of Q-CdS. These values are summarized in Table 3-2.

Table 3-2 The particle size distribution of Q-CdS obtained by TEM.

D[a] / Å	f[b]	v[c] /10^{20} cm^3	f × v /10^{21} cm^3
14	0.004	0.14	0.006
18	0.008	0.31	0.025
22	0.045	0.56	0.251
26	0.078	0.92	0.716
30	0.117	1.41	1.659
34	0.136	2.06	2.808
38	0.124	2.87	3.567
42	0.091	3.88	3.546
46	0.072	5.10	3.685
50	0.055	6.54	3.572
54	0.049	8.24	4.049
58	0.078	10.2	7.944
62	0.035	12.5	4.426
66	0.031	15.1	4.723
70	0.018	18.0	3.185
74	0.035	21.2	7.526
78	0.018	24.8	4.407
82	0.004	28.9	1.182
	1.000		Σ f×v = 57.28

a D:diameter

b f: Frequency of the size distribution of Q-CdS obtained by TEM.

c v: particle volume = $\pi D^3 / 6$

Applying $\Sigma f_i v_i = 5.73 \times 10^{-20}$ (cm^3) which is obtained from Table 3-2 and V_0 of 5.4×10^{-3} (eq. 3-4) to eq. 3-5, N is determined to be 9.4×10^{16} (particle cm^{-3}). On the other hand, the number of Q-CdS particles which survived after the photocorrosion process with irradiation of monochromaticlight can be estimated based on the concentration of initially existed Q-CdS particles and the amount of sulfate ions resulted from the photocorrosion provided that the size distribution of Q-CdS is nearly monodispersed . In that case, the number of particles present in the unit volume of solution is given by

$$n = \frac{1.8\times10^{-4} - [SO_4^{2-}]}{\pi/6 \times (D\times10^{-8})^3\times4.82} \qquad (3\text{-}6)$$

where n is the number of particles (number dm^{-3}), 1.8×10^{-4} (mol dm^{-3}) the original concentration of Q-CdS, D (Å) the diameter of Q-CdS particles obtained by applying the first exciton peak energy to the finite depth potential well model. $[SO_4^{2-}]$ (mol dm^{-3}) is the concentration of sulfate ions produced by eq. 3-3

The number of Q-CdS particles obtained by eq. 3-6 are decreased with increasing the excitation wavelength as shown in Figure 3-7. Based on the relation between the number of Q-CdS particles and excitation wavelength given in this figure, the absorption coefficient at the first exciton peak was estimated using eq. 3-7.

$$\varepsilon = \frac{A_{exciton}}{N / 6.02 \times 10^{23}} \qquad (3\text{-}7)$$

where N is the number of Q-CdS particles in the colloids, ε is the absorption coefficient, $A_{exciton}$ is the absorbance at the first exciton peak, and 6.02×10^{23} is the avogadro number. The results obtained are also included in Figure 3-7.

Figure 3-7 clearly shows that ε was independent of the particle sizes. This

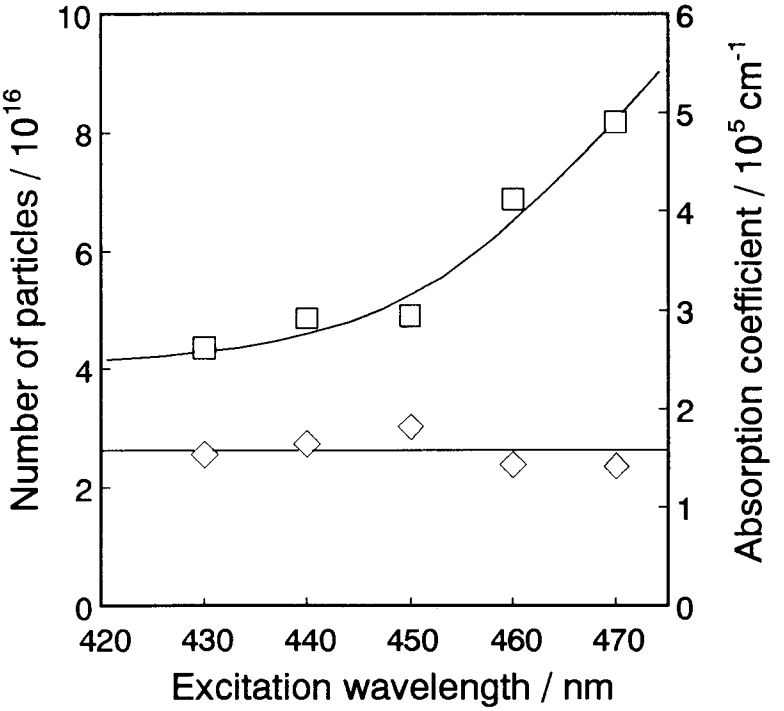

Figure 3-7 The number of the particles (□) present in Q-CdS colloids and the absorption coefficient (◇) of the Q-CdS colloids, obtained by photocorrosion as a function of the excitation wavelength used in the photocorrsion.

results agree well with the previously reported results of the size independence of the absorption coefficient.[14] These facts indicate that the estimation of the particle number of Q-CdS using the sulfate ions (eq. 3-6) are reasonable.

3-4 References

1 Recent reviews: for example (a) Steigerwald, M. L.; Brus, L. E. *Annu. Rev. Mater. Sci.* **1988**, *19*, 471; (b) Henglein, A. *Chem. Rev.* **1989**, *89*, 1861; (c) Wang, Y.; Herron, N. *J. Phys. Chem.* **1991**, *95*, 525; (d) Weller, H. *Angew. Chem. Int. Ed. Engl.* **1993**, *32*, 41.

2 For example: (a) Wang, Y.; Herron, N. *J. Phys. Chem.* **1987**, *91*, 257; (b) Abe, T.; Tachibana, Y.; Uematsu, T.; Iwamoto, M. *J. Chem. Soc., Chem. Commun.* **1995**, 1617.

3 Yoneyama,;H, Haga, S.; Yamanaka, S. *J. Phys. Chem.* **1989**, *93*, 4833.

4 For example: (a) Meyer, M.; Wallberg, C.; Kurihara, K.; Fendler, J. H. J. *Chem. Soc., Chem. Commun.* **1984**, 90; (b) Lianos, P.; Thomas, J. K. *Chem. Phys. Lett.* **1986**, *125*, 299; (c) Petit, C.; Pileni, M. P.; *J. Phys. Chem.* **1988**, *92*, 2282; (d) Nosaka, Y.; Yamaguchi, K.; Miyaha, H.; Hayashi, H. *Chem. Lett.* **1988**, 605; (e) Kortan, A. R.; Hull, R.; Opila, R. L.; Bawendi, M. G.; Steigerwald, M. L.; Carroll, P. J.; Brus, L. E. *J. Am. Chem. Soc.* **1990**, *112*, 1327. (f) Rajh, T.; Micic, O. I.; Nozik, A. J. *J. Phys. Chem.* **1993**, *97*, 11999;

5 For example: H. Miyoshi, M. Yamachika, H. Mori, H. Yoneyama *J. Chem. Soc., Faraday, Trans.*, **1990**, *86*, 815.

6 (a) Fisher, Ch.-H.; Weller, H.; Fojtik, A.; Lume-Pereira, C.; Janata, E.; Henglein, A. *Ber. Bunsen-Ges. Phys. Chem.* **1986**, *90*,46; (b) Fisher, Ch.-H.; Weller, H.; Katsikas, L. and Henglein, A. *Langmuir*, **1989**, *5*, 429; (c) Fisher, Ch.-H.; Lilie, J.; Weller, H.; Katsikas, L.; Henglein, A. *Ber. Bunsen-Ges. Phys. Chem.* **1989**, *93*, 61.

7 Wang, Y.; Harmer, M.; Herron, N. *Israel J. Chem.* **1993**, *33*, 31.

8 Murray, C. B.; Norris, D. J.; Bawendi, M. G. *J. Am. Chem. Soc.* **1993**, *115*, 8706.

9 Vossmeyer, T.; Katsikas, L.; Giersig, M.; Popovic., I. G.; Diesner, K.; Chemseddine, A.; Eychmüller, A.; Weller, H. *J. Phys. Chem.* **1994**, *98*, 7665.

10 (a) Weller, H.; Koch, U.; Gutiérrez, M.; Henglein A. *Ber. Bunsen-Ges. Phys. Chem.* **1984**, *88*, 649; (b) Spanhel, L.; Haase, M.; Weller, H.; Henglein, A. *J. Am. Chem. Soc.* **1987**, *109*, 5649.

11 Lippens, P. E.; Lanoo, M. *Phys. Rev. B* **1989**, *39*, 10935.

12 Nosaka, Y. *J. Phys. Chem.* **1991**, *95*, 5054.

13 a) Meissner, D.; Memming, R.; Shuben, L.; Yesodharan, S.; Grätzel, M. *Ber. Bunsen-Ges. Phys. Chem.*, **1985**, *89*, 121; (b) Meissner, D.; Memming, R.; Kastening, B. *J. Phys. Chem.*, **1988**, *92*, 3476.

14 Hanamura, E. *Phys. Rev. B* **1988**, *37*, 1273.

Chapter 4 Photoinduced Reaction on Quantized GaAs Nanocrystals Prepared by Wet Process

4-1 Introduction

So far a variety of semiconductor nanocrystals have been synthesized, but they belong mostly to II-VI compound semiconductors such as CdS and ZnS, or oxide semiconductors such as TiO_2 and Fe_2O_3.

It is expected that III-V compound semiconductors such as GaAs and InP show large quantum size effects because of very small effective mass of an electron and a hole. But the preparation of the III-V semiconductor nanocrystals is not so easy as that of II-VI semiconductor nanocrystals. InP nanocrystals were successfully prepared in zeolite cages[6]. As for GaAs nanocrystals, they have mostly been prepared using dry process such as MOCVD and molecular beam epitaxy[7-8], which require the use of expensive instruments. In addition, the size of the prepared particles were widely dispersed.

Recently, Alivisatos *et al* [9] and Uchida *et al* [10-11] successfully synthesized GaAs nanocrystals under mild conditions using wet processes in which organometallic reactions in organic solvents were employed. The prepared GaAs colloids exhibited activities for transient photobleaching in picosecond laser pump-probe experiments[11]. Also reported was a large third-order nonlinearity in the degenerative four-wave mixing experiments[12]. However, detailed investigations on photoinduced electron transfers have not yet been reported. GaAs nanocrystals would be an interesting material as a photocatalyst, because GaAs has very good matching to the solar spectrum.

In this chapter, photoinduced reduction of methylviologen in GaAs nanocrystals prepared by the same method as that reported by Uchida *et al* [11] is reported in reference to the reduction behaviors on bulk GaAs particles.

4-2 Experimental Section

The following chemicals were used as received; Gallium(III) acetylacetonate ($Ga(acac)_3$) (Strem Chemicals), ammonium hexafluorophosphate (Aldrich), bulk GaAs powder (CERAC), methylviologen dichloride (Tokyo Kasei) and 2-mercaptoethanol (Wako Pure Chemicals). Tris(trimethylsilyl) arsine ($As(SiMe_3)_3$) was prepared according to the literature[13] and purified by vacuum distillation. Methylviologen was used as a hexafluorophosphate salt, which was prepared by reacting the dichloride salt with NH_4PF_6. Triethylene glycol dimethylether (triglyme) was purchased from Aldrich and distilled over CaH_2 under reduced pressure (~10 Torr). Acetonitrile was from Wako Pure Chemicals and distilled over P_2O_5 under N_2 atmosphere.

The preparation of GaAs nanocrystals, which is denoted Q-GaAs, was followed to that prepared by Uchida *et al* [11]. 25 cm^3 of triglyme containing 0.5 mmol of $Ga(acac)_3$ and 0.5 mmol of $As(SiMe_3)_3$ was heated at reflux temperature (216) for 70 hours, resulting in brown slurries, which was filtered through a 0.2μm-PTFE filter (Advantec) to remove bulky solids. Transparent orange GaAs colloids were obtained as a filtrate. By applying the orange colloids to ultrafiltration using AMICON YM1 (average pore size = 1.2 nm), Q-GaAs colloids were obtained. As a blank sample, triglyme containing the same concentration of $Ga(acac)_3$ alone was heated under the same conditions. All manipulations were performed in a vacuum chamber under oxygen free dry nitrogen atmosphere.

A transmission electron microscope, TEM (Hitachi, H-800, 200 kV) was employed to estimate the size distributions. For this purpose, a small amount of the Q-GaAs colloid (0.2μm filtrate) was dropped onto carbon-evaporated copper grids, followed by drying.

The amount of gallium and arsenic contained in the GaAs nanocrystals were determined using a fluorescent X-ray spectrometer (RIGAKU, 3270A). As the standard samples, known amounts of Ga and As atomic absorption standard solutions

(Wako Pure Chemicals) were dropped onto filter papers (RIGAKU, 3379C1), followed by drying under vacuum. In the concentration range of the calibration (~1000 ppm), matrix effect was negligible.

Optical absorption spectra of the Q-GaAs colloid were measured with use of a Hewlett Packard 8452A UV/Vis photodiode array spectrophotometer. The optical path length chosen was 2 mm.

The photoinduced reduction of methylviologen (MV^{2+}) on the Q-GaAs was investigated in the following way. To 3.5 cm^3 of acetonitrile containing 2-mercaptoethanol as a hole scavenger and MV^{2+} as an electron acceptor, 0.5 cm^3 of the Q-GaAs colloid which contain 0.42 μmol of Q-GaAs was added, and the resulting solution was deaerated by bubbling nitrogen for 20 minutes. As a reference 4.0 cm^3 of acetonitrile containing 2-mercaptoethanol and MV^{2+} of the same concentration and 13 μmol of bulk GaAs powder was prepared. The second harmonic (532 nm) of a Q-switched Nd:YAG laser (Spectra-Physics, GCR-11, pulse width: 7 ns, beam intensity: 10~100 mJ per pulse) was irradiated onto the acetonitrile solution contained in a 1 cm × 1 cm quartz cell with frequency of 10 Hz. The photoinduced formation of $MV^{+\cdot}$ was monitored by measuring changes in absorption at 606 nm using the photodiode-array spectrometer.

4-3 Results and Discussion

4-3-1 Observation of Q-GaAs by TEM

The formation of GaAs nanocrystals were confirmed by observations with TEM and electron diffraction patterns. The electron diffraction patterns simultaneously obtained with observations by TEM were hkl zinc blende patterns of (200) (220) (400) (331) of GaAs only and no other pattern was seen. Figure 4-1 shows a TEM picture of the prepared Q-GaAs, where GaAs particles ranging from 1.5 nm to 9.0 nm are seen. If the size distribution of the Q-GaAs was obtained

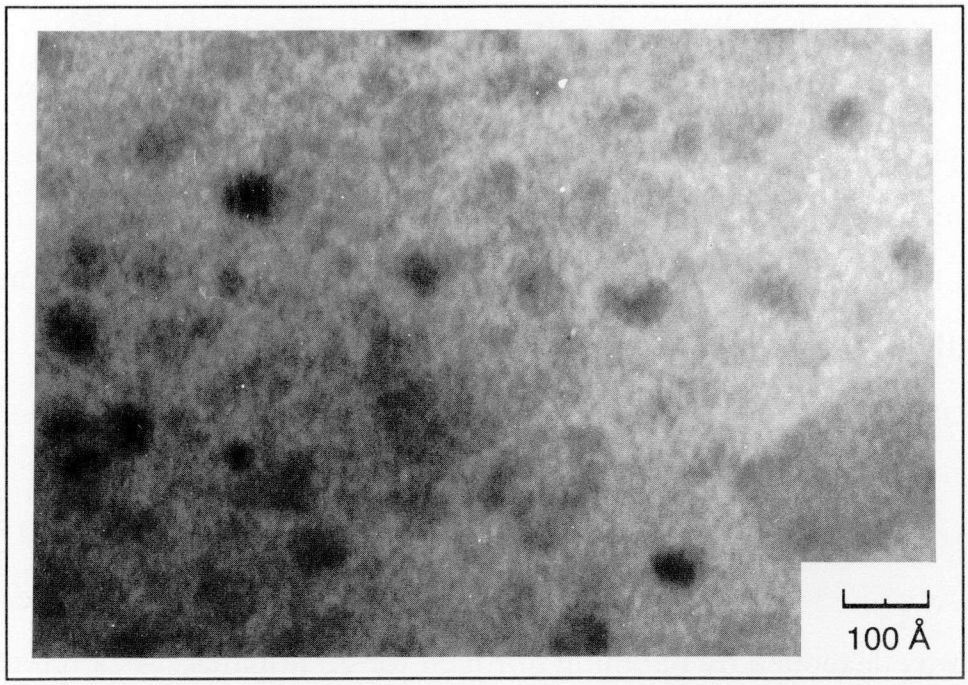

Figure 4-1 TEM image of Q-GaAs. For preparation conditions: See text.

for several TEM pictures, the results shown in the inset of the Figure 4-2 were obtained. The average diameter and standard deviation was 4.5 nm and 1.59 nm, respectively.

4-3-2 Optical Absorption Spectra of Q-GaAs Colloid

The optical absorption spectra of Q-GaAs colloid is given by a spectrum (a) of Figure 4-2, and that of the blank sample prepared by refluxing triglyme in the presence of $Ga(acac)_3$ is by spectrum (c) of the same figure. There are marked difference between these two spectra. It is believed that the blank sample contained gallium-triglyme-acetylacetonate complexes, because triglyme is a good complexing agent for many metals[14]. However it was not possible to isolate the complex as a solid from the blank sample. When the Q-GaAs colloid was subjected to ultrafiltration using a 1.2 nm pore size filter to remove the GaAs nanocrystals, the resulting filtrate gave spectrum (b) of Figure 4-2, which is similar to that of the blank sample. Accordingly it is highly probable that the Q-GaAs colloid contained gallium-triglyme-acetylacetonate complexes. If 700 nm was chosen as the

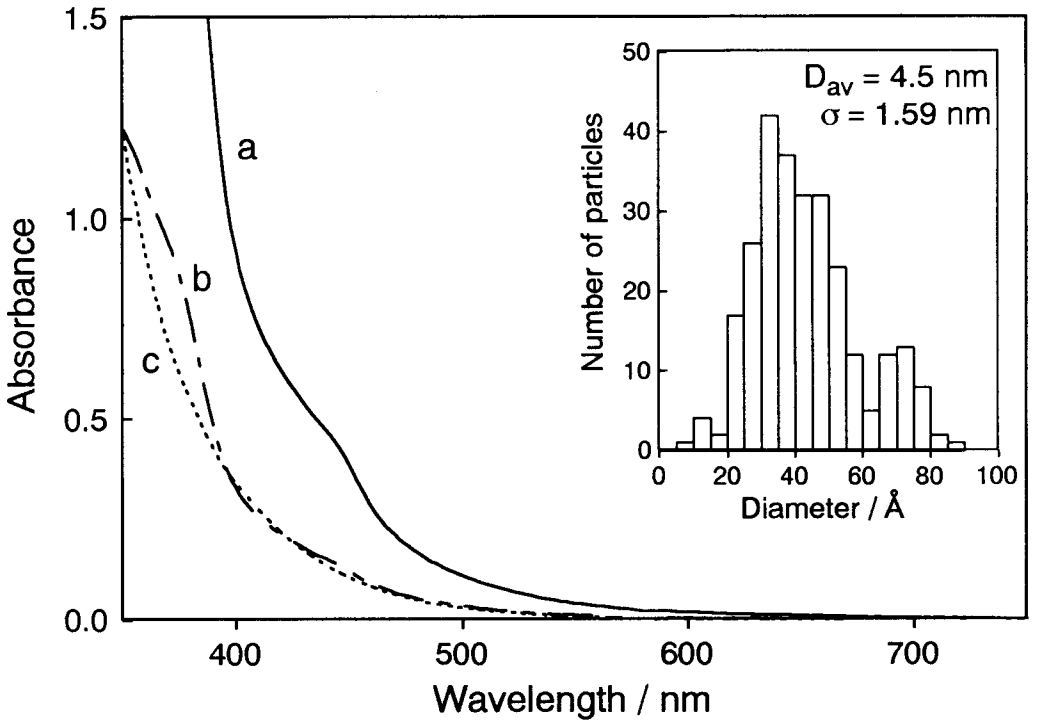

Figure 4-2 Absorption spectra of Q-GaAs colloid filtered through 0.2 μm- (a) and 1.2 nm- (b) pore size filters. A spectrum of the $Ga(acac)_3$-triglyme blank solution filtered through 0.2 μm filter (c) is also shown. Optical path length = 2 mm. Inset shows that size distributions of Q-GaAs determined from TEM image. The total number of particles counted was 270. The average diameter is 4.5 nm with the standard deviation of 1.59 nm.

absorption onset of spectrum (a) of Figure 4-2, then 1.77 eV was obtained as the band gap energy of the prepared GaAs nanocrystals, giving 0.25 eV extension of the bandgap of bulk crystal due to the quantum size effects. Several papers have been published on the relationship between the diameter of semiconductor particle and bandgap energy[15-18]. If the relation derived by Wang *et al*[16] was used to estimate the bandgap of the largest GaAs particles present in the colloids, 1.77 eV is obtained, which is in good agreement with the absorption threshold of spectrum (a) of Figure 4-2. Considering that the absorption threshold is determined by the largest particles present in semiconductor colloids[19], the result seems reasonable.

4-3-3 Determination of Gallium and Arsenic Contained in the Q-GaAs

The Q-GaAs colloids were subjected to ultrafiltration with the use of 1.2 nm

Table 4-1 Concentration of Ga and As Contained in 0.2μm- and 1.2nm-filtrates of the GaAs Colloid Determined by Fluorescent X-ray Analysis

No.	Sample	Gallium (mmol dm^{-3})	Arsenic (mmol dm^{-3})
1	loaded[a]	20	20
2	0.2μm-filtrate	7.20	1.32
3	1.2nm-filtrate	3.04	0.48
4	Δ(2-3)[b]	4.16	0.84

[a] Original concentration of the starting materials.
[b] Difference between the run No.2 and 3, corresponding to the composition of GaAs nanocrystals greater than 1.2 nm.

pore size filter. By the filtration, the Q-GaAs must be eliminated from the filtrate as judged from the particle distribution (see inset of the Figure 4-2). The amount of gallium and arsenic contained in the resulting filtrate was determined by fluorescent X-ray spectrometry. The results are summarized in Table 4-1. In this table, results obtained prior to the filtration are included. The colloidal filtrate obtained by filtration with a 0.2 μm filter of the triglyme solution after reaction of $Ga(acac)_3$ with $As(SiMe_3)_3$ contained 36 % of gallium and 6.6 % of arsenic of the loaded amount used in the preparation of the GaAs particles. The difference in the concentration between No. 2 and No. 3 which is shown in No. 4 of the Table 4-1 must be related to the Q-GaAs particles which were retained on a 1.2 nm filter. As Figure 4-2 shows, the size of the GaAs particles left on the 1.2 nm filter ranged from 1 nm to 9 nm. There was no GaAs particles having the size greater than 10 nm, though the colloidal sample applied to the filtration with 1.2 nm filter was prepared by filtration with a 0.2 μm filter. The amount of gallium given in No. 4 of the Table 4-1 was about four times as large as that of arsenic, suggesting that some gallium species other than GaAs existed on the filter. The species were not detected by electron diffraction analysis. If it is assumed that all the arsenic contained in the colloid prepared by filtration with 0.2 μm filter were involved in the formation of GaAs particles, 0.84 mmol dm^{-3} of GaAs is obtained. As recognized from the

results shown in Table 4-1, 20 % of gallium that was contained in the colloids prepared by filtration with 0.2 μm filter was utilized in the preparation of GaAs particles. The rest was left on the filter, probably as gallium-triglyme-acethylacetonate complexes. Some of them may have existed on GaAs particles as adsorbates and some of them may not but were left on the filter due to too bigness to be filtered. Unfortunately, it was difficult to isolate the complexes from the GaAs particles to determine their chemical compositions and to identify the substances.

4-3-4 Photoinduced Electron Transfer on Q-GaAs

Photocatalytic activities of the Q-GaAs colloids were examined for photoreduction of MV^{2+} whose redox potential in acetonitrile is -0.45 V vs sce [20]. The bulk GaAs has a reducing power large enough to reduce MV^{2+}; its flatband potential in acetonitrile is reportedly -1.0 V vs SCE [21]. The Q-GaAs particles must have a higher reducing power than the bulk GaAs due to the size quantization effect. Irradiation with 532 nm laser beam of an 3.5 cm^3 of acetonitrile solution containing 0.5 cm^3 of the Q-GaAs colloid, which contained 60.8 μg (= 0.84 mM × 0.5 cm^3 × 144.6 g mol^{-1}) of GaAs nanocrystals, 0.1 mol dm^{-3} 2-mercaptoethanol as a hole scavenger, and 5 mmol dm^{-3} MV^{2+}, resulted in an intense absorption at 606 nm, which was due to methylviologen cation radical ($MV^{+\cdot}$, ε_{606} = 13700 mol^{-1} dm^3 cm^{-1})[22] formation. The photoinduced reduction reactions of MV^{2+} are given by eq. 4-1~4-3.

$$GaAs + h\nu \rightarrow e^- + h^+ \quad (4\text{-}1)$$

$$e^- + MV^{2+} \rightarrow MV^{+\cdot} \quad (4\text{-}2)$$

$$h^+ + HSCH_2CH_2OH \rightarrow {}^{\bullet}SCH_2CH_2OH + H^+ \quad (4\text{-}3)$$

The photoreduction of MV^{2+} was also observed for a bulk GaAs powder in the same acetonitrile solution, as expected. Increase in the absorption at 606 nm with

irradiation time is given in Figure 4-3 both for the Q-GaAs colloids and for the bulk GaAs powder. It is seen that in both kinds of GaAs, the absorbance increased linearly with irradiation time. If the initial rate of $MV^{+\cdot}$ production per milligram of photocatalyst, which is denoted r_{init} (μmol sec^{-1} mg^{-1}), was determined from the slope of the absorbance change under different illumination intensities, results shown in Figure 4-4 were obtained. The initial reduction rate of MV^{2+} increased roughly in proportion to the illumination intensity both for the Q-GaAs and for the bulk GaAs powder, suggesting that the concentration of excited electrons in the conduction band of GaAs determined the rate of photoreduction of MV^{2+}. The rate equation is then given by eq. 4-4 if the reduction rate of MV^{2+} under a fixed illumination intensity is proportional to the concentration of MV^{2+}, too.

$$e^- + MV^{2+}_{ads} \xrightarrow{k} MV^{+\cdot} \qquad r_{init} = k[MV^{2+}_{ads}][e^-] \tag{4-4}$$

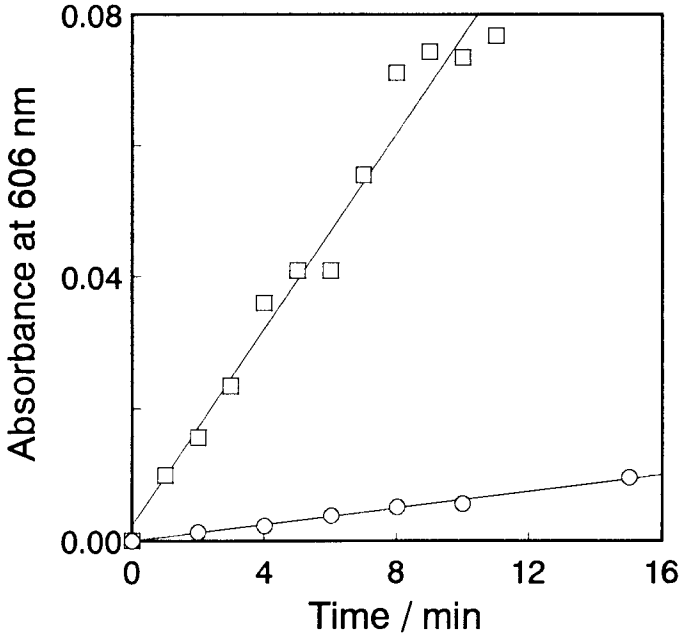

Figure 4-3 Absorbance change at 606 nm caused by laser irradiation. (O) Q-GaAs (60.8 μg), and (□) bulk GaAs (1.9 mg). $[MV^{2+}]$= 5 mmol dm^{-3}, [2-mercaptoethanol] = 0.1 mol dm^{-3}. Laser power = 50 mJ per pulse. The Q-GaAs colloid which contained Ga-complexes was used to prepare the MV^{2+} solution contain Q-GaAs.

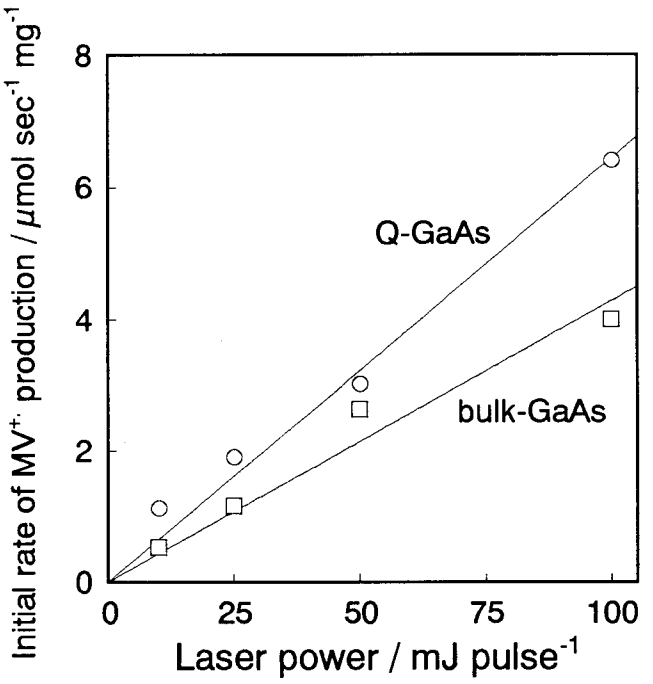

Figure 4-4 Dependence of the initial rate of $MV^{+\cdot}$ production on laser power. (O) Q-GaAs, (□) bulk GaAs. The experimental conditions: As in Figure 4-3, but for various illumination intensities.

Figure 4-5 shows the effect of the concentration of MV^{2+} on the initial rate of its photoreduction. The intensity of the laser beam was 50 mJ per pulse. It is seen

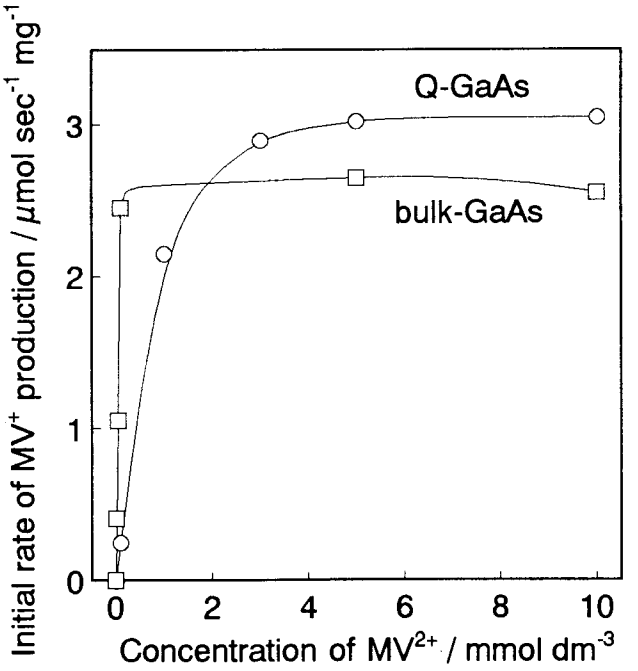

Figure 4-5 The effect of MV^{2+} concentration on the initial rate of $MV^{+\cdot}$ production. (O) Q-GaAs, (□) bulk GaAs. Laser power = 50 mJ per pulse. [2-mercaptoethanol]= 0.1 mol dm^{-3}.

that r_{init} was easily saturated with increasing the MV^{2+} concentration, and 3.0 μmol sec^{-1} mg^{-1} was obtained as a saturated r_{init} for the Q-GaAs colloids, while 2.5 μmol sec^{-1} mg^{-1} for the bulk GaAs powder. Considering that photoinduced reduction of MV^{2+} takes place on the semiconductor particle surfaces, it seems reasonable to discuss the reduction rate of MV^{2+} for unit surface area of the semiconductor particles. The surface area of Q-GaAs and bulk GaAs particles used in this experiments were estimated as follows. The Q-GaAs particles had a size distribution as shown in the inset of the Figure 4-2. With illumination at 532 nm, a fraction of Q-GaAs can be photoexcited. If the threshold particle diameter is evaluated using the equation derived by Wang *et al* [16], it is concluded that GaAs particles of 4.8 nm or the larger can respond to this illumination. By taking the size distribution of Q-GaAs particles given in the inset of the Figure 4-2 into account, the total surface area of the Q-GaAs above 4.8 nm employed in the experiments (60.8 μg) is estimated to be 85 cm^2, that is, 1398 cm^2 per milligram of Q-GaAs. The mean diameter of the bulk GaAs was determined by using a dynamic light scattering apparatus (Photal DLS-700) to be 0.4 μm. Then the total surface area of bulk GaAs particles used in the experiment (1.9 mg) was estimated to be 14 cm^2, that is, 7.4 cm^2 per milligram of bulk GaAs. By using these surface areas, the initial MV^{2+} reduction rate for the unit area (r_{init}') was obtained as shown in Table 4-2.

Table 4- 2 The Initial Rate of $MV^{+\cdot}$ Production on Q-GaAs and Bulk GaAs

	W[a] /mg	S[b] /cm^2mg^{-1}	N_{ph}[c] /photon sec^{-1}	r_{init} /μmol $sec^{-1}mg^{-1}$	r_{init}'[d] /μmol $sec^{-1}mg^{-1}cm^{-2}$	η[e] /%
Q-GaAs	0.0608	1398	7.4×10^{16}	3.0	0.0021	0.15
bulk GaAs	1.9	7.4	8.0×10^{17}	2.5	0.34	0.36

[a] W : Weight of the photocatalyst employed in the experiments.
[b] S :Total surface area per milligram of photocatalyst which can absorb 532 nm laser beam.
[c] N_{ph} : the number of absorbed photons calculated from absorbance at 532 nm.
[d] $r_{init}' = r_{init} / S$
[e] η : quantum efficiency for $MV^{+\cdot}$ production at 532 nm. $\eta(\%) = r_{init} \times W \times 10^{-6} \times 6.02\times10^{23} / N_{ph}$

The obtained r_{init}' of the Q-GaAs was smaller than that for the bulk GaAs. Usually, a higher reduction rate is expected for the quantum sized semiconductor photocatalyst due to its higher reducing power, being in contradiction with the experimental finding. It is then thought that a poor adsorbability of MV^{2+} onto the Q-GaAs surfaces may be responsible for the observed poor activity of the Q-GaAs photocatalysts. To get information about this, attempts were made to determine the apparent association constant between MV^{2+} and GaAs particles by analyzing the dependence of r_{init} on the MV^{2+} concentration which is given in Figure 4-5. If the Langmuir adsorption equilibrium establishes between MV^{2+} and GaAs particles, eq. 4-5 must be valid.

$$\theta^{-1} = 1 + (K_{app}[MV^{2+}])^{-1} \qquad (4\text{-}5)$$

where θ is the surface coverage of MV^{2+} and K_{app} is an apparent association constant. If it is assumed that the reduction rate is given by eq. 4-4, the rate is linearly proportional to the amount of adsorbed MV^{2+} under a fixed illumination intensity. Then in a concentration range of MV^{2+} which gives the constant reduction rate (r_{sat}), the methylviologen must be adsorbed on GaAs particles with a full coverage. If this assumption is valid, the surface coverage θ is given by the ratio of the reduction rate obtained under various concentrations to the constant rate ($\theta = r/r_{sat}$). Using θ values obtained in this way, θ^{-1} vs $[MV^{2+}]^{-1}$ plots were made. As shown in Figure 4-6, the results given in Figure 4-5 satisfy well eq. 4-5 for both kinds of photocatalysts. From the gradients of the plots shown in Figure 4-6, K_{app} of the bulk GaAs was obtained to be 1.9×10^4 $mol^{-1}dm^3$, while that for the Q-GaAs was 9.3×10^2 $mol^{-1}dm^3$, the former being 20 times as large as that for the latter.

Why the adsorbability of MV^{2+} on the Q-GaAs particles was very low compared to that on the bulk GaAs particles is a matter for discussion. As suggested from the results shown in Table 4-1, the Q-GaAs used in the photoreduction experiments of MV^{2+} contained gallium-triglyme-acac complexes. If the complexes

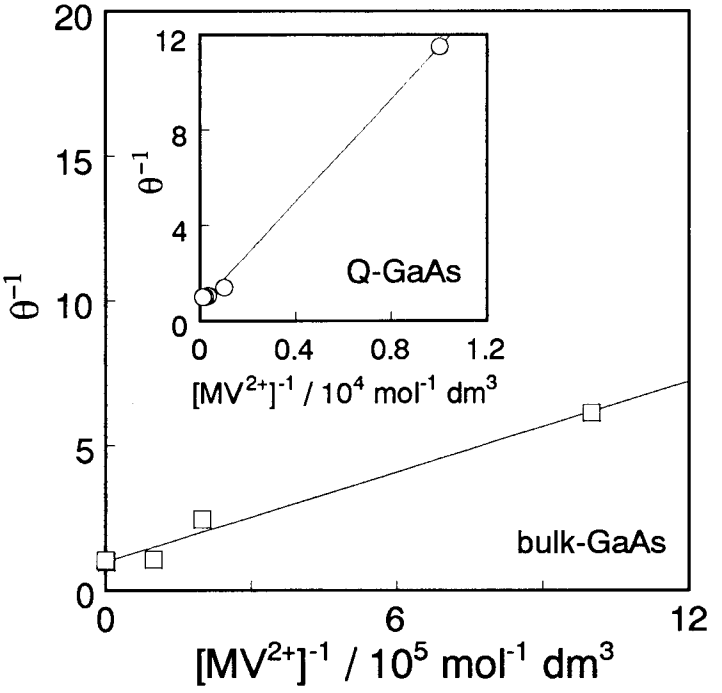

Figure 4-6 Plot of θ^{-1} vs. $[MV^{2+}]^{-1}$. (O) Q-GaAs, (□) bulk GaAs.

adsorb on the Q-GaAs particle surfaces, they must hinder the photoinduced charge transfer reactions on the semiconductor particles. Cyclic voltammetry of the blank sample prepared by refluxing triglyme in the presence of $Ga(acac)_3$ revealed that the blank sample was electrochemically inactive in acetonitrile. Since it is believed that the blank sample contained Ga-triglyme-acethylacetonate complexes, the complexes must be electrolytically inactive. Consequently, the poor photocatalytic activities of Q-GaAs must be caused by blocking effects of the Ga-complexes for adsorption of MV^{2+} onto GaAs particles, though it is not known how greatly the GaAs particles are blocked by the Ga-complexes. Anyway, the existence of the adsorbed Ga-complexes makes the comparison of the photocatalytic activities of the Q-GaAs with those of bulk GaAs insignificant. Since the Ga-complexes work as stabilizing agents for GaAs particles, it is not easy to remove the complex from the GaAs particles as long as the present preparation methods are concerned. Then it will be of significance to investigate another means of the preparation of Q-GaAs that allows detailed characterization of the particles surfaces. The preparation on inert solid supports, for example, may be of great value toward this direction.

4-4 References

1 Steigerwald, M.L., and Brus, L.E. *Acc. Chem. Res.* **1990**, *23*, 183.

2 Wang, Y., and Herron, N. *J. Phys. Chem.* **1991**, *95*, 525.

3 Henglein, A. *Chem. Rev.* **1989**, *89*, 1861.

4 Weller H. *Angew. Chem. Int. Ed. Engl.* **1993**, *32*, 41.

5 Kamat, P.V. *Chem. Rev.* **1993**, *93*, 267.

6 Uchida, H., Ogata, T. ,and Yoneyama, H. *Chem. Phys. Lett.* **1990**, *173*, 103.

7 Wang, Y., and Herron, N. *Res. Chem. Intermed.* **1991**, *15*, 17.

8 Sandroff, C.J., Harbison, J.P., Ramesh, R., Andrejco, M.J., Hegdg, M.S., Hwang, D.M., Chang, C.C., and Vogel, E.M. *Science* **1989**, *245*, 391 .

9 Olshavsky, M.A., Goldstein, A.N., and Alivisatos, A.P. *J. Am. Chem. Soc.* **1990**, *112*, 9438.

10 Uchida, H., Curtis, C.J., and Nozik, A.J. *J. Phys. Chem.* **1991**, *95*, 5382.

11 Uchida, H., Curtis, C.J., Kamat, P.V., Jones, K.M., and Nozik, A.J. *J. Phys. Chem.* **1992**, *96*, 1156.

12 Matsumoto, H., Uchida, H., Sakata, T., Mori, H., Sasaki, T., and Yoneyama, H. *Denki Kagaku* **1993**, *61*, 918.

13 Becker, G., Gutekunst, G., and Wessely, H.J. *Z. Anorg. Allg. Chem.* **1980**, *113*, 462.

14 Van Gils, N., Zuur, A.P., and Driessen, W.L. *Inorg. Chim. Acta* **1982**, *58*, 187.

15 Brus, L.E. *J. Chem. Phys.* **1983**, *79*, 5566.

16 Wang, Y., Suna, A., Mahler, W., and Kasowski, R. *J. Chem. Phys.* **1987**, *87*, 7315.

17 Lippens, P.E., and Lannoo, M. *Phys. Rev. B* **1989**, *39*, 10935.

18 Nosaka, Y. *J. Phys. Chem.* **1991**, *95*, 5054.

19 Weller, H.,Schmidt, H.M., Koch, U., Fojtik, A., Baral, S.,Henglein, A., Kunath, W., Weiss, K., and Diemann, E. *Chem. Phys. Lett.* **1986**, *124*, 557.

20 Osa, T., and. Kuwana, T *J. Electroanal. Chem.* **1969**, *22*, 389

21 Kohl, P.A, and Bard, A.J. *J. Electrochem. Soc.* **1979**, *126*, 59.

22 Watanabe, T., and Honda, K. *J. Phys. Chem.* **1982**, *86*, 2617.

Conclusion

This thesis have dealt with quantitative analysis of the size effect of photocatalytic properties of semiconductor nanocrystals and with the development of the preparation method of monodispersed semiconductor nanocrystals. The main results and conclusions obtained in this study are summarized as follows.

In chapter 1, it is described that photoinduced reduction of methylviologen on quantized CdS nanocrystals conducted with pulsed laser irradiation at 355 nm occurred under activation control of electrochemical reactions. The higher reduction rate was obtained at the smaller particles, reflecting a general trend in electrochemical reduction that an increase in the potential difference between the conduction band of CdS nanocrystals and methylviologen favors the photoinduced charge transfer between them. On the other hand, reduction of propyl-viologensulfonate was found to occur under diffusion control which obscured effects of particle size effect if any. Such difference in the reduction behavior of the two kinds of viologens results from differences in their adsorbability onto CdS nanocrystals. Evidences supporting this view were obtained from fluorescence quenching and transient absorbance experiments of CdS nanocrystal colloids.

In chapter 2, it is described that the analysis of fluorescence quenching based on adsorption-desorption equilibrium between CdS nanocrystals and TiO_2 colloids allowed the determination of the conduction band potential of CdS nanocrystals and the estimation of surface hydroxylation of CdS nanocrystals which takes place in solutions with pH greater than 10. The electron transfer from CdS nanocrystals to TiO_2 colloids occurs under activation control and its rate depends on the potential difference in the conduction bands between the two kinds of semiconductors.

In chapter 3, it is described that a size distribution of polydispersed CdS nanocrystals whose average diameter was 42 Å and standard deviation was 19 Å

was narrowed by using size selective photocorrosion which was achieved by sequential irradiation with monochromatic light whose wavelength was changed step by step from 490 to 430 nm in air-saturated sodium hexametaphosphate solution. With decrease in the wavelength of irradiated light, the first exciton peak was gradually developed in the absorption spectrum of the resulting CdS nanocrystal colloids.

In chapter 4, it is described that GaAs nanocrystals prepared in the present study exhibited large quantum size effects. Being contrary to the expectation, the photocatalytic activity of the GaAs nanocrystals for reduction of methylviologen was lower than that of bulk GaAs particles. Ga-complexes and/or organic species which acted as stabilizing agents for the GaAs nanocrystal adsorbed on the GaAs particles, and hindered the adsorption of methylviologen. In order to have exact information on the photocatalytic activities of GaAs nanocrystals, it is necessary to prepare GaAs nanocrystals having well defined surface structures. Researches toward this direction will be of great significance.

Acknowledgment

The work of this thesis was carried out under the guidance of Professor Dr. Hiroshi Yoneyama at Department of Applied Chemistry, Faculty of Engineering, Osaka University.

The author would like to express his grateful acknowledgement to Professor Dr. Hiroshi Yoneyama for his continuous guidance and encouragement throughout this work.

The author is also indebted to Professor Dr. Gin-ya Adachi for his helpful comments and suggestions.

The author is very grateful to Associate Professor Dr. Susumu Kuwabata and Lecturer Dr. Tsukasa Torimoto for their impressive instruction and suggestions.

The author desired to express his sincere thanks to Associate Professor Dr. Hiroyuki Uchida, Yamanashi University, and Lecturer Dr. Hiroshi Inoue, University of Osaka Prefecture for many useful suggestions for performing this study.

The author makes grateful acknowledgement to Professor Dr. Hirotaro Mori and Dr. Takao Sakata, Research Center for Ultra-High Voltage Electron Microscopy, Osaka University for their collaborations and useful discussion.

The author wishes to thank his co-workers, Mr. Takahiro Matsunaga, Mr. Hiroshi Yamauchi, Mr. Masahide Miyake, Mr. Syuji Satoh, and all other member of the Yoneyama Laboratory for their kind help.

Finally, the author is particularly grateful to his parents and sister, Tsukasa Matsumoto, Eiko Matsumoto, Junko Matsumoto for their hearty encouragements, understandings , and perpetual support.